https://doi.org/10.5194/egusphere-2026-4185
Preprint. Discussion started: 27 July 2026

Evaluating hysteresis mechanisms through pore networks simulations

Ilan Ben-Noah[1], Shmulik P. Friedman[1], and Yechezkel Mualem[2]

[1]Department of Environmental Physics and Irrigation, Institute of Soil, Water and Environmental Sciences, The Volcani Institute, Agricultural Research Organization, Rishon LeZion, Israel
[2]Department of Soil and Water Sciences, The Hebrew University of Jerusalem, Rehovot, Israel

Correspondence: Ilan Ben-Noah (ilanb@volcani.agri.gov.il)

Abstract.

Hysteresis in capillary head and relative permeability relationships with saturation degree is an important phenomenon in granular and porous media. Accounting for hysteresis is essential for accurately predicting flow in multiphase systems in hydrological applications such as groundwater management and soil water dynamics. The observed hysteresis loops reflect complex, history-dependent interactions between fluids and pore structures. This work uses three-dimensional (3D) pore network models to systematically investigate how media properties. We analyse the influence of the pore size distribution, correlation, and connectivity on the combined and decoupled mechanisms causing hysteresis: geometric ink bottle effects, non-wetting fluid trapping, and network-dependent effects arising from complex pore accessibility.

By leveraging controlled simulated drainage and imbibition scenarios, namely invasion vs random percolation, bond vs site-governed displacement, and with vs without trapping, we decoupled these mechanisms. The different mechanisms present distinct effects on the hysteretic loops. In particular, trapping primarily affects retention curves at high saturation degrees of the wetting phase (S_w) and dramatically reduces wetting-phase relative permeability (k_r^W). In comparison, the ink-bottle effect, driven by pore geometry, is visible across the entire capillary head (h_c) range. In contrast, network hysteresis effects significantly the shape of the retention curve ($S_\mathrm{w}(h_\mathrm{c})$) loops and drives $k_\mathrm{r}(S_\mathrm{w})$ hysteresis at low S_w.

Furthermore, the impact of these mechanisms is highly dependent on medium structure. Increasing the spread of the pore size distribution enhances non-wetting phase trapping volume while mitigating ink bottle effects. Correlation between pore bodies' and throats' radii strongly increases the impact of trapping on k_r^W. Conversely, increasing connectivity (i.e., higher coordination number) reduces the trapped fluid fraction and generally mitigates ink bottle and network hysteresis effects in retention evaluation. These results provide necessary mechanistic understanding, supporting the inverse interpretation of hysteretic loops to deduce the underlying topological structure of porous media.

1 introduction

Undersatnding the different governing mechanism and media properties affecting hysteresis in capillary head and relative permeability dependence on saturation degree is essential for accurately predicting multiphase flow. The shapes and behaviors of the hysteresis loops, whether they close neatly, cross over, or exhibit horizontal plateaus or immediate sharp changes, are direct consequences of the complex, history-dependent interactions between fluids and pore structures at the pore level (Jerauld

https://doi.org/10.5194/egusphere-2026-4185
Preprint. Discussion started: 27 July 2026

and Salter, 1990). These interactions hold information regarding the pore size distribution and pore system connectivity. For example, Knackstedt et al. (1998, 2001) showed that to quantitatively fit experimental mercury porosimetry data, the effect of correlations between the sizes of pore throats must be taken into account, implying that deviations in the hysteresis loop can reveal information about these correlations. Liu et al. (1993a, b) suggested levaraging sorption-desorption hysteretic loops curves to evaluate the pore size distribution and mean coordination number of the pore system. Jerauld and Salter (1990) utilized a pore-level model to simulate hysteresis in relative permeability and capillary head. They found that the pore-body to pore-throat aspect ratio strongly influences the shape of hysteresis loop. The connection between mercury porosimetry hysteresis and percolation theory is well recognized (Chatzis and Dullien, 1977; Larson et al., 1981b; Wall and Brown, 1981). This relation implies that mechanistic pore network models can provide a framework for which the specific shapes of hysteresis loops can be linked back to fundamental features like pore size distribution, pore body-throat aspect ratio, and connectivity.

However, a deeper understanding is crucial on the the individual and combined roles of the differnet mechanisms that casues hysteresis, namely the effect of the geometric ink-bottle effects, the trapping of non-wetting fluid, and network effects arising from complex pore accessibility. This comprehensive understanding is necessary to enable the inverse interpretation of hysteretic loops (from measurements such as capillary head or relative permeability dependence on saturation degree) to accurately deduce the underlying topological structure and other intrinsic properties of the porous medium.

This work uses three-dimensional (3D) pore networks to investigate the effects of the media properties and fluid invasion modes on the hysteresis in the retention and relative permeability curves. Namley, the effect of the pore size distribution, network connectivity (topology), and pore geometry correlations on the different mechanisms is analyzed by leveraging different simulated drainage and imbition scenarios that account for different physical displacement processes. The displacement processes differes in the filling order of the pores (i.e., imbibibtion or drainage), the phase accesability (i.e., random vs invasion percolation), the governing curvature (site vs bond displacement), and with or without trapping of the residing phase. This allows for a systematic evaluation of the combined and separated (decoupled) effects of the different hysteretic mechanisms, which cannot be evaluated in experimental studies.

This work is organized as follows: first, a brief introdactory section is presented that describes the various quasi-static hysteretic mechanisms (1.1), followed by a discussion on using pore network models (1.2) to evaluate the two-phase distribution within the context of these different hysteretic mechanisms in the retention and permeability curves (1.3). Next, the methods section (2) presents the pore networks used in this study and the different evaluated displacement scenarios. Then, the results and discussion section (3) systematically presents the combined and decoupled effects of the different hysteresis mechanisms (3.1), and in comparison the intercorrelated effects of: pore size distributions (3.2), correlation between pore bodies and throats (3.3), and network connectivity and regularity (3.4), on hysteresis in the retention and relative permeability curves.

1.1 Hysteresis mechanisms

Different types of hysteretic curves visually represent the history-dependent relationships between system variables (Preisach, 1935). The Néel-Everett (Everett, 1955; Néel, 1942) independent domain model provides the theoretical framework for describing the various hysteretic curve types (Topp, 1969). The independent domain theory assumes that hysteresis at each pore (element)

https://doi.org/10.5194/egusphere-2026-4185
Preprint. Discussion started: 27 July 2026

is independent of its neighbors. In addition, this theory assumes that a hysteretic relationship is independent of time. This can be considered as a good approximation of actual phenomena in which changes occur in a time interval long enough to approach a state of quasi-equilibrium, but short enough to avoid relaxation phenomena (such as air dissolution and diffusion) (Mualem, 1974). The distinctive shape of the main loop, which serves as the signature of hysteresis (Mualem, 1974), is the enclosed area between two curves: (i) The main drainage curve (or drying curve) traces the system's response as a state variable (e.g., water content) decreases from its maximum value (e.g., saturation); (ii) The main imbibition curve (or wetting curve) illustrates the system's response as the state variable increases back to its maximum. Within the main hysteretic loop, scanning curves represent intermediate paths taken when the direction of change in the external (prescribed) variable is reversed before the system reaches the full limits of the main loop. These curves form smaller, nested loops within the larger main loop (Topp, 1969). A distinct type of curve is the first drainage curve, which represents the initial drainage from a completely saturated sample. This curve can differ from subsequent main drainage curves, often influenced by phenomena such as entrapped air that prevents the system from reaching its absolute maximum saturation upon rewetting (Poulovassilis, 1970).

There are three major hysteretic mechanisms during capillary equilibrium (quasi-static) displacement:

1. *"Ink-bottle hysteresis"* is a geometric phenomenon that arises from the irregular, non-uniform cross-sections of pores (Haines, 1930; Mualem, 1973; Sahimi, 2011), like an ink bottle with a narrow neck and a wider body, for which the imbibition is according to the radius (curvature) of the wider body and the drainage is according to the neck's radius.

2. *Trapping* of the non-wetting (NW) fluid, particularly during imbibition. As the wetting phase invades, portions of the NW fluid can become disconnected and immobile, forming isolated clumps or ganglia within the pore network. This trapped fluid cannot be displaced by further changes in capillary head (Jerauld and Salter, 1990; Poulovassilis, 1970).

3. *Network hysteresis*, or dependent-domain hysteresis (Mualem, 1984), is fundamentally a process driven by the complex connectivity and accessibility of pores in the medium. Thus, this process can be conceptualized as a percolation process (Chatzis and Dullien, 1977; Hunt and Sahimi, 2017). The way fluids penetrate and are distributed within the pore network, and thus the resulting clusters of occupied pores, differ between drainage and imbibition. This is because the accessibility of pores to a fluid depends on the surrounding pore structure and the saturation history, causing distinct pathways to form and leading to different saturation–capillary head relationships during fluid advance versus retreat.

1.2 Two-phase quasi-static displacement in pore networks

The theory of evaluating two-phase fluid distribution and hydraulic properties using pore networks involves representing the complex geometry and topology of porous media as an interconnected network of pore-bodies and pore-throats (Blunt, 2017; Fatt, 1956; Jerauld and Salter, 1990; Sahimi, 2011). This network model, which mimics the essential features of the pore space relevant to fluid flow, approximates the description of the pore space and fluid movement using a small set of parameters and simple rules (Jerauld and Salter, 1990; Sahimi, 2011).

Pore network models can be constructed through simple regular lattices of capillary elements or by modeling the stochastic topology directly, often using techniques like X-ray computed tomography (Sahimi, 2011). Simulating two-phase fluid distribu-

https://doi.org/10.5194/egusphere-2026-4185
Preprint. Discussion started: 27 July 2026

tion within this network involves modeling a sequence of pore-level events, such as invasion during drainage and snap-off or retraction during imbibition (Avraam and Payatakes, 1995; Blunt, 2017; Hunt and Sahimi, 2017; Sahimi, 2011). These events are governed by capillary forces and depend on the connectivity and wettability of the fluids and solid (Ben-Noah et al., 2023; Sahimi, 2011). For example, drainage processes where the non-wetting phase (NWP) invades are often simulated as **Invasion Percolation (IP)** (Lenormand et al., 1983; Wilkinson and Willemsen, 1983; Wilkinson, 1986). IP requires a continuous pathway of occupied bonds (or sites), from the invasion source to the bond (/site) under consideration. In contrast, the wetting phase (WP) imbibition processes are often described as a **Random Percolation (RP)**. RP assumes that the invading phase percolates to the pores by the filling order (decreasing in size for the NWP and increasing for the WP) regardless of their location on the grid. This is justified by the accessibility of each pore to the wetting phase through film flow (Hunt and Sahimi, 2017). The different modes of percolation for drainage and imbibition relate to the network hysteresis mechanism (see mechanism 3 in the above subsection), e.g., a large pore surrounded by small pores is "protected" from drainage via IP but not via RP.

In this context, **trapping** forms one of the major differences between drainage and imbibition (see mechanism 2 in the above subsection), as it is strongly suppressed by corner flow of the residing (defender) W phase during drainage. IP can be described as “with” or “without” trapping of the residing phase by the invading phase (Sahimi, 2011; Wilkinson, 1984). As the occupation probability of the invading phase increases, differences between RP and IP decrease, while differences between IP with and without trapping increase. Trapping is also possible in RP, for which most properties with or without trapping are the same (Dias and Wilkinson, 1986).

Moreover, imbibition is often conceptualized as a **site displacement** process, driven by the filling of pore bodies. As opposed to Imbibition site displacement, the narrower **bond displacement** controls the non-wetting (NW) invasion (drainage), by the resistance of capillary forces (Butcher, 1975; Chatzis and Dullien, 1977; Jarrell, 2002; Koplik, 1982; Reis and Måløy, 2025; Sahimi et al., 1998). In this analogy, pore bodies are represented as "sites" (or "vertices" in topological terminology) and pore throats as "bonds" (or "hedges") within the network model (Blunt, 2000; Dias and Payatakes, 1986; Koplik et al., 1988). This difference relates to the Ink bottle hysteresis mechanism (see mechanism 1 in the above subsection).

1.3 Retention and permeability curves

Once the microscopic fluid distribution is established, macroscopic hydraulic properties, i.e., capillary head (retention) and relative permeability are evaluated. It is commonly assumed that the phase-filled pore bodies determines the media retention while the throats determine the resistance to the flow (relative permeability). Capillary pressure, defined as the equilibrium pressure difference between the non-wetting and wetting phases, is directly related to the two-phase interface geometry (curvature), which is shaped by phase configurations and the pore network’s geometry (Blunt, 2017). Under equilibrium conditions, capillary pressure (or head when divided by the W phase specific weight, $\rho_w g$) can be evaluated using simplified interface geometry (curvature) via the Young-Laplace equation (Fatt, 1956). Network models, often leveraging percolation theory, have been used to compute capillary head/saturation degree relationships, for instance, in mercury porosimetry curves (Chatzis and Dullien, 1985).

Relative permeability is calculated by treating each fluid phase as a separate sub-network of interconnected pore elements. This approach builds upon foundational work by Fatt (1956) and has been extensively developed (Heiba et al., 1992; Jerauld

https://doi.org/10.5194/egusphere-2026-4185
Preprint. Discussion started: 27 July 2026

and Salter, 1990; Mohanty and Salter, 1982). These calculations involve assigning hydraulic conductances to these fluid sub-networks, and solving mass balance equations to determine fluid flux. The entire process of two-phase flow and its resulting hydraulic properties is frequently understood as a percolation phenomenon, where fluid connectivity and accessibility are critical for flow pathways to span the network (Heiba et al., 1992; Hunt and Sahimi, 2017; Larson et al., 1981b). In simple geometry networks, the bond conductance can be estimated using Hagen-Poiseuille (Poiseuille, 1839) law (e.g. for cylindrical bonds, Fatt (1956)).Under steady-state conditions, the relative permeability of a sample-spanning phase can be evaluated by solving Kirchhoff laws, that is, a set of homogeneous linear equations.

2 Methods

In this section, first, the construction of the pore networks with different properties is described. Next, the different displacement rules, accounting for different hysteresis mechanisms, are discussed. Finally, a critical discussion about the proposed methodology and analysis is presented.

2.1 Pore networks

2.1.1 Networks description

This study considers a simple-cubic pore network array composed of bonds and sites, which relate, in accordance, to the pore throats and bodies. Conceptually, the bonds' geometry is taken to be cylindrical, while the sites, which are located at the junctions, are spherical. In this simplification, the resistance to the flow is attributed only to the bonds and the volume of the two fluids occupying the pore system, only to the sites

$$V_T = \frac{\Sigma_i^{N_s} V_{s,i}}{n} \tag{1}$$

where V_T is the total volume of the domain, the porosity of the domain is set constant to $n = 0.38$ (typical to granular media, e.g. a packing of sand grains), $V_{s,i} = \frac{4\pi r_{s,i}^3}{3}$, where $V_{s,i}$ is the volume and $r_{s,i}$ is the radius of site i, N_s is the number of sites, which for a parallelepiped holds $N_s = N^3$, where N is the lattice (network) size.

The number of sites in this analysis ($N_s = 15^3 = 3,375$) is chosen to balance computation times and acceptable bias caused by the bounded (finite-size) domain. The effect of the finite domain is evaluated through a sensitivity analysis. The sensitivity analysis and measures taken to reduce the bias effect of the limited domain are presented in Appendix A. The effect of the small lattice is mitigated and evaluated by using three repetitions (realizations) for each lattice.

The domain size (equal in all directions) is determined from the total volume of the sites (V_T) and the porosity.

$$L_x = L_y = L_z = L = V_T^{1/3}, \tag{2}$$

where L_z, L_y, and L_x [L] are the height, width, and length of the cubic domain.

https://doi.org/10.5194/egusphere-2026-4185
Preprint. Discussion started: 27 July 2026

This determines the bond lengths ($\ell = L/N$ [L]), which correspond to the distance between the centers of the sites (i.e., including the two sites' radii). The conductance (κ [$\mathrm{M^{-1}L^4T}$]) of a cylindrical tube is given by Poiseuille (1839)

$$\kappa = \frac{\pi r_\mathrm{b}^4}{8\mu_\alpha \ell}, \tag{3}$$

where r_b [L] is the cylinder radius, μ_α [$\mathrm{ML^{-1}T^{-1}}$] the α fluid's dynamic viscosity (with $\alpha = W$ or NW for the wetting and non-wetting phases, in accordance). The pore flow rate [$\mathrm{L^3T^{-1}}$] is $Q_b = \kappa|\Delta p|$, where Δp [$\mathrm{ML^{-1}T^{-2}}$] is the pressure drop along the length ℓ of the pore. It should be noted that the absolute value of ℓ does not affect any the relative permeability or retention curves.

2.1.2 Pore size distribution

The pore size distribution (PSD) strongly affects the magnitude and shape of the hysteresis loop (Assouline and Rouault, 1997). In the synthetic media presented here, a log-normal PSD is assumed (Friedman and Seaton, 1996) for both the pore bodies and throats. In this, the radii of the sites (r_s) and bonds (r_b) are randomly sampled from a PSD

$$r_k = \frac{{\mu_k}^2}{\sqrt{{\mu_k}^2 + {\sigma_k}^2}} exp[n\sqrt{ln(1 + {\sigma_k}^2/{\mu_k}^2)}] \tag{4}$$

where n is a random number drawn from a normal distribution, subscript k refers to either site (s) or bond (b), μ_k [L] is the mean, and σ_k [L] is the standard deviation.

The mean pore body is $\mu_s = 5 \cdot 10^{-3}\ cm$ and the mean throat radius $\mu_b = 2.5 \cdot 10^{-3}\ cm$. Three levels of variability in the pore size distribution are analysed. The different spread in the PSD is categorized with different standard deviations (σ) of coefficient of variation of $CV = 0.2$, 0.5, and 1 for the "low", "medium", and "high" variability, respectively. Figure 1 presents the different pore size distributions used for the different variabilities (and for the three realizations).

It should be emphasized that using a single size (r_s) to characterize both the volume of the pore and its capillary head is a simplification of the real-world complex pore shape geometry. Similarly, the bond's radius (r_b) should not be considered the actual size of the aperture between real media pore bodies, but rather a representative radius of its conductance (κ, following Eq. 3).

2.1.3 Correlated pore bodies and throats

In addition to the variability in the PSD, the correlation between the pore bodies' and throats' radii may also play a significant role in the different mechanisms of hysteresis (Heiba et al., 1992). In general, one might expect that large pore bodies will also have large throats (and vice versa). However, this is not necessarily the case. Here, the geometrical mean of neighboring pore bodies ($\sqrt{r_{s,i} \cdot r_{s,j}}$) is used to correlate the radii of the bodies and throats. In this, the throats' radii are assigned in the same order as that of the geometrical mean of the pore bodies connected by the throat, that is, the k^{th} largest r_b is assigned to the connection with the k^{th} highest geometrical mean of r_s. For the Not-correlated case, the spatial distribution of r_s was kept as that for the mutual correlated network (for each realization), while the same set of r_bs was reassigned randomly (Figure 2).

https://doi.org/10.5194/egusphere-2026-4185
Preprint. Discussion started: 27 July 2026

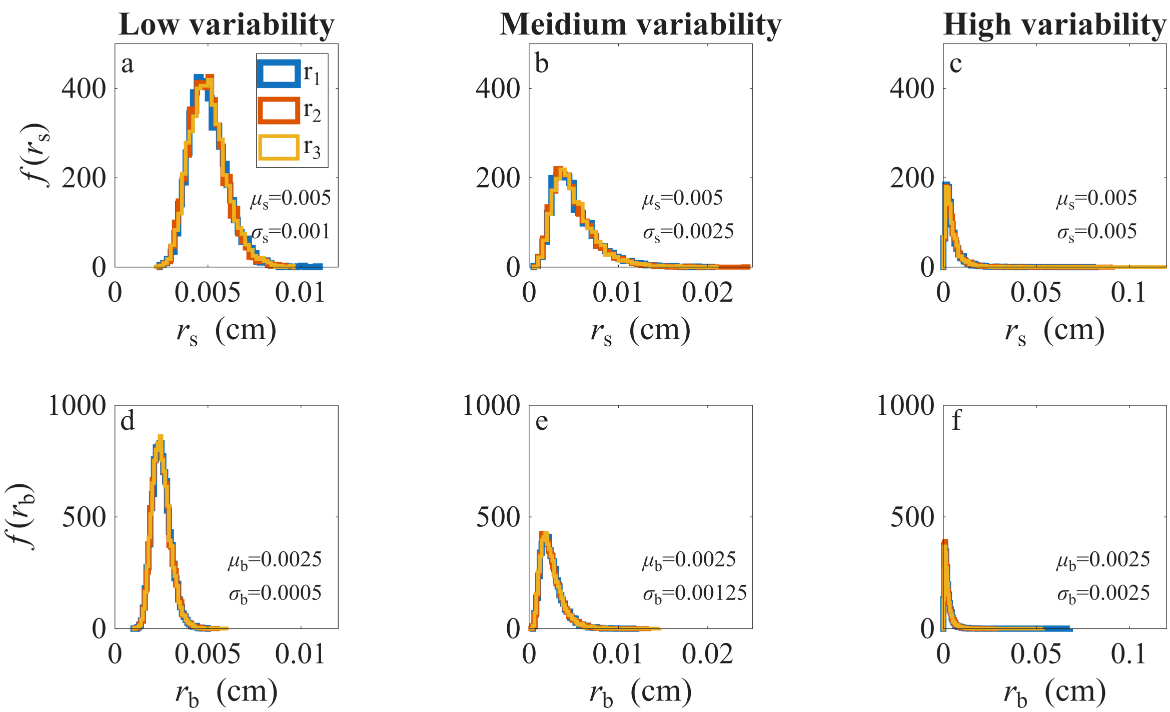

Figure 1. Probability density functions of the pore bodies $(a-c)$ and throats $(d-f)$ size distributions for the low $(a\&d)$, medium $(b\&e)$, and high $(c\&f)$ variability of the different realizations $(r_1, r_2,$ and $r_3)$.

2.1.4 Network connectivity

The network connectivity is of major significance to the hysteresis mechanisms, especially for the trapping (mechanism 2, in the list above) and network hysteresis (3) mechanisms. As described above, a simple cubic (SC) array, with a coordination number $N_\mathrm{c} = 6$ is considered at the basis of this work. Two aspects of network connectivity are then evaluated:

i) The effect of the coordination number is evaluated by running the same simulations on a regular lattice that includes also the Face-diagonal neighbors, that is, the nearest (NN) and the 2nd nearest (2NN) neighbors ($N_\mathrm{c} = 18$) (Figure 3a).

ii) The effect of the lattice regularity (3D topology beyond N_c) is evaluated by running the same simulations on an irregular lattice with a quasi-normal distribution of the number of connections and a similar mean coordination number ($\bar{N}_\mathrm{c} = 6$). Similarly to the correlation between r_s and r_b, one may expect larger pores to have more connections than smaller pores. In this analysis, two cases are considered: with (Figure 3c) and without (Figure 3b) correlation between the pore body size (r_s) and its number of connections (N_c).

The quasi-normal (discrete) distribution of connections is obtained by drawing N_s numbers from a distribution of integers (N_c) between 1 and 18 with a probability given by

https://doi.org/10.5194/egusphere-2026-4185
Preprint. Discussion started: 27 July 2026

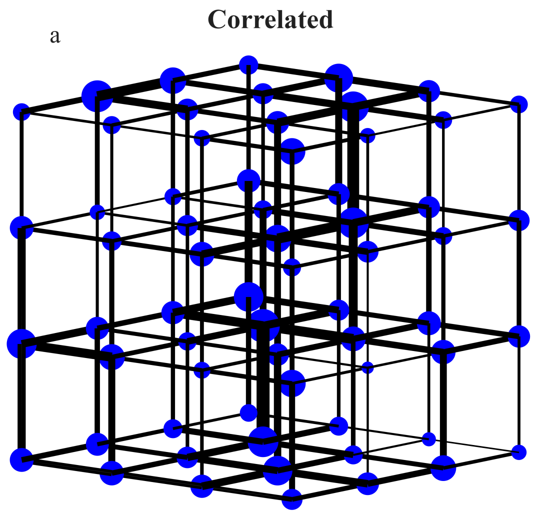

Figure 2. Schematic description of a section of the network with (a) and without (b) correlation between the sites and the bond radii. The spheres represent the pore bodies and the cylinders the throats. The diameters of the spheres and cylinders are, in accordance, proportional to r_s and r_b, but not in scale to the actual simulated sizes or to the ratio between the sites and bond radii.

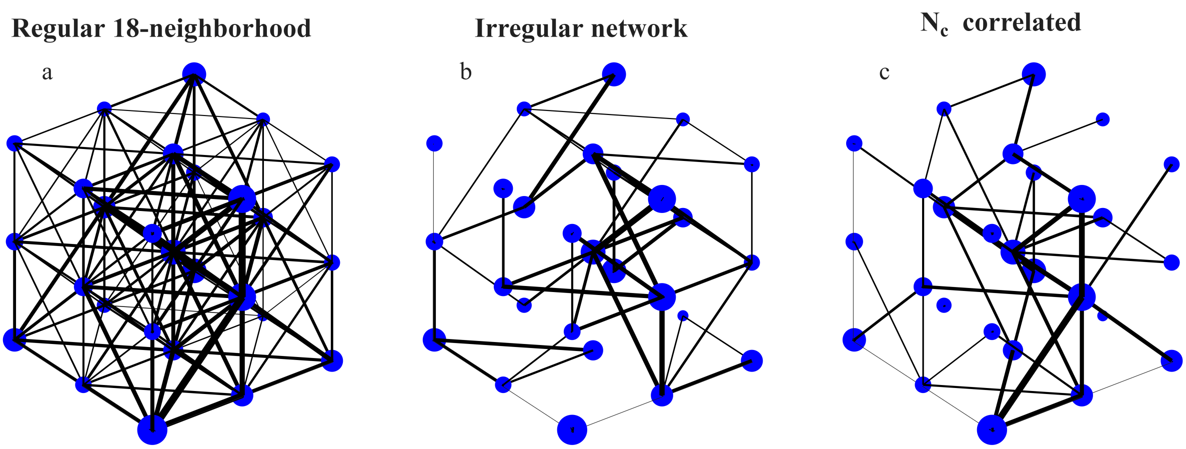

Figure 3. Schematic description of a section of (a) regular 18-neighborhood network (simple cubic array with NN+2NN), (b) irregular network with a mean coordination number $\bar{N}_\mathrm{c} = 6$, and (c) the same irregular pore distribution with $\bar{N}_\mathrm{c} = 6$, but with also correlation between the local N_c and the pore size. The spheres represent the pore bodies and the cylinders the throats. The diameters of the spheres and the cylinders are, in accordance, proportional to r_s and r_b, but not in scale to the actual simulated sizes or to the ratio between the sites and bond radii.

$$p(N_c) = \frac{e^{-\frac{1}{2}((N_c-\bar{N}_\mathrm{c})/\sigma)^2}}{\sum_{N_c=1}^{18} e^{-\frac{1}{2}((N_c-\bar{N}_\mathrm{c})/\sigma)^2}}, \tag{5}$$

where $\sigma = 2$ was chosen as the standard deviation of the coordination numbers distribution.

https://doi.org/10.5194/egusphere-2026-4185
Preprint. Discussion started: 27 July 2026

To create the irregular network, the procedure described in Ben-Noah et al. (2024a) is used. This process iterates both dilution and concentration processes using a target number of connections to each site and an elimination number to each bond of the saturated (completely filled) lattice. We start from a regular 18-neighborhood lattice, i.e., with a constant coordination number of $N_c = 18$. This value equals the largest allowable number of connections. Adjusting the distribution of coordination numbers of the lattice to a prescribed distribution is done iteratively through diluting and concentrating schemes. First, the algorithm is initialized by assigning a target number of connections $\mathbb{N}_\mathrm{c} \leq 18$ to each site. For the case where N_c is not correlated with the pore size, $\mathbb{N}_\mathrm{c}$ are drawn randomly from the distribution $p(N_c)$ (Eq. 5). For the correlated case, the $\mathbb{N}_\mathrm{c}$ are ranked and assigned so that the k^{th} largest $\mathbb{N}_\mathrm{c}$ is assigned to the k^{th} largest site (r_s). In addition, for the N_c-coorrelated case, the reciprocal of the connected sites geometrical mean ($\frac{1}{\sqrt{r_{s,i} \cdot r_{s,j}}}$) is taken to equal the bond elimination number, while for the not-correlated case the elimination number is drawn randomly from a uniform distribution between 0 and 1. All site coordination numbers at initialization are $N_c^{(0)} = 18$. We start with a dilution step, if a site coordination number is larger than the target value ($N_c^{(0)} > \mathbb{N}_c$), the bond with the smallest elimination number is removed by assigning zero conductance. After the dilution step, all coordination numbers are updated. The dilution step is followed by a concentration step. If the grid coordination number at the site is smaller than the target value ($N_c^{(1)} < \mathbb{N}_c$), then a bond is added (to one of the available locations) and a new random elimination number is assigned to the bond. After the concentration step, all coordination numbers are updated, and a dilution step follows. These steps are repeated until the distribution of coordination numbers in the irregular network has converged to the target distribution. As a convergence criterion, we use a threshold value for the difference between the target and lattice mean coordination number. That is, the algorithm has converged after the kth iteration if $|\langle \mathbb{N}_c \rangle - \langle N_c^{(k)} \rangle| < 10^{-4}$. Once the lattice converges, the bond radii (r_b) are assigned based on the geometrical mean of the sites as described in the above subsection.

2.2 Displacement processes and hysteresis mechanisms

Up to this point, the technical details of the network construction and the media properties to be analyzed have been described. This section presents and discusses the different displacement rules considered and their relation to the corresponding hysteretic mechanisms.

The different scenarios are categorized by:

1. the main process, i.e, **Imbibition** or **Drainage**.
2. the governing geometry of displacement, i.e, **Site** or **Bond**.
3. the percolation mode, i.e, **Random** or **Invasion** percolation.
4. the trapping of the resident phase, i.e, with **Trapping** or **No-trapping**.

2.2.1 Combined effects of hysteresis mechanisms

As discussed above in the theory section, the WP imbibition is expected to follow a site-random percolation with trapping of the residing NWP (ISRT, in table 1), while the drainage with the invading NW-phase displacing the WP is expected to follow a

https://doi.org/10.5194/egusphere-2026-4185
Preprint. Discussion started: 27 July 2026

Acronym	Displacement	Site/Bond	Percolation mode	Trapping
ISRT	**I**mbibition	**S**ite	**R**andom	**T**rapping
DBIN	**D**rainage	**B**ond	**I**nvasion	**N**o-trapping
I/DSRN	Reversible	**S**ite	**R**andom	**N**o-trapping
ISIN	**I**mbibition	**S**ite	**I**nvasion	**N**o-trapping
DSIN	**D**rainage	**S**ite	**I**nvasion	**N**o-trapping
ISIT	**I**mbibition	**S**ite	**I**nvasion	**T**rapping

Table 1. Different displacement models acronyms and processes.

bond-invasion percolation without trapping of the WP (DBIN, in table 1). In contrast to this hysteretic loop, which combines the different mechanisms, the imbibition or drainage through random percolation without trapping (I/DSRN) is the "ideal" filling of the pores from the smallest to largest (imbibition) or the other way around (drainage). These processes are not hysteretic, that is, they are completely reversible (ISRN≡DSRN, see table 1). In addition to these basic scenarios, here we also modeled a set of "degenerated" physical cases in order to systematically evaluate the role of the different mechanisms and their interaction with the different media properties. This type of systematic analysis, decoupling the different hysteresis mechanisms, cannot be achieved experimentally.

Table 1 lists the six models (hysteretic displacement modes) evaluated in this work (and their acronyms). Each of these scenarios was evaluated with different media properties: i) pore size variability (low, medium, and high), ii) pore size correlation (with and without), iii) connectivity (regular $N_\mathrm{c} = 6$, regular $N_\mathrm{c} = 18$, irregular $\bar{N}_\mathrm{c} = 6$, and irregular $\bar{N}_\mathrm{c} = 6$ with correlation to the pore size), simulating three realizations (total of 126 simulations).

2.2.2 Trapping

The decoupled effect of trapping can be evaluated by comparing ISRT to I/DSRN or ISIT to ISIN scenarios. The differences between these comparisons are attributed to the effects of the percolation mode (IP or RP) on the trapping of the residing phase. As further discussed below in the Limitations section, here we regard the residing phase to be trapped if it is not connected to any of the lattice external faces, including the ones that are perpendicular to the flow direction. This definition of trapping underestimates the role of trapping compared to impermeable perpendicular faces.

2.2.3 Ink bottle hysteresis

Ink bottle hysteresis is directly related to the differences between site and bond displacement processes. The drainage through site-governed displacement (DSIN) basically assumes that the pores invaded by the NWP are controlled by the capillary resistance to the expulsion of the WP rather than by the invasion of (their accessibility to) the NWP. This process neglects the ink-bottle hysteresis mechanism. Thus, this decoupled effect can be evaluated by comparing the DBIN to DSIN scenarios. The bond/site-displacement should not be confused with the bond/site-percolation, where the former refers to the curvature of the

https://doi.org/10.5194/egusphere-2026-4185
Preprint. Discussion started: 27 July 2026

meniscus governing the displacement, and the latter refers to the network occupation. This work considers only site-percolation, that is, the bonds connecting two sites with the same phase are immediately occupied with this phase, regardless of the process (i.e., "imbibition" or "drainage") or the meniscus' curvature governing the displacement (i.e., "bond" or "site"). This is in accordance with the assumption that the bonds have no volume (see discussion above regarding the radius r_b compared to the actual aperture between pores). These automatically invaded bonds contribute to the permeability (k_r) of the pore network to the invading phase, but do not affect the evaluated capillary head, which corresponds to the displaced bond (the largest accessible one) in the DBIN scenario. Another important clarification is that using the bond radius (r_b) to evaluate the capillary head in the DBIN case assumes that the radius (determining the conductance) equals the curvature radius (related to the actual aperture through Young-Laplace), which is not necessarily the case. This assumption underestimates the actual pore aperture, thus overestimates the effect of the ink bottle (widening the hysteretic loop). Despite that, these radii (of the actual aperture and r_b) are strongly correlated, thus the qualitative analysis is not expected to be affected by this (common) inconsistency.

2.2.4 Network hysteresis

The IP differs from the RP mode mostly by the "acceptance profile' (Wilkinson and Willemsen, 1983), which is the range of pore sizes that are accepted in the cluster. In this, the RP has a sharp profile while the IP has a transition zone allowing for a filling order different than the "ideal" (I/DSRN) one. In other words, in the IP mode, the pores are not necessarily filled in increasing or decreasing order, but rather depend on the accessible pores at the front. When, for example, during drainage, a smaller pore is drained before a larger one, the corresponding capillary head remains the one that was attained to drain the smaller one. This process is related to the network hysteresis, as small pores surrounding a larger one are "protecting" it from being drained, for example. This mechanism is related to the "dependent domain" approach (Mualem, 1974; Mualem and Dagan, 1975; Mualem and Miller, 1979; Mualem, 1984; Topp, 1971). Comparing the imbibition (ISIN) and drainage (DSIN) through the IP mode allows the evaluation of the effect of this mechanism on the hysteretic loop.

Figure 4 presents the spatial pores and throats filled with the invading phase at breakthrough for the different modes. The number fraction of filled pores at breakthrough is termed the percolation threshold (p_{cs}). Comparing the ISRT (panel "a" in figure 4) to ISIT (panel f) demonstrates the differences between random and invasion percolation where the number of filled pores in ISRT is ca. 3-fold larger. However, despite this difference in p_{cs} the differences in the commutative volume of the invaded spheres is less significant compared to the differences when comparing DSIN (panel e) and ISIN (panel d), that is, the filling order affects the saturation more than the p_{cs}. The insignificant effect of trapping at breakthrough is visible when comparing ISIN (d) and ISIT (f). This observation holds for also ISRT (a) and ISRN (not presented), Keep in mind that DSRN (c) at breakthrough is also the disconnection point of the residing phase during ISRN.

https://doi.org/10.5194/egusphere-2026-4185
Preprint. Discussion started: 27 July 2026

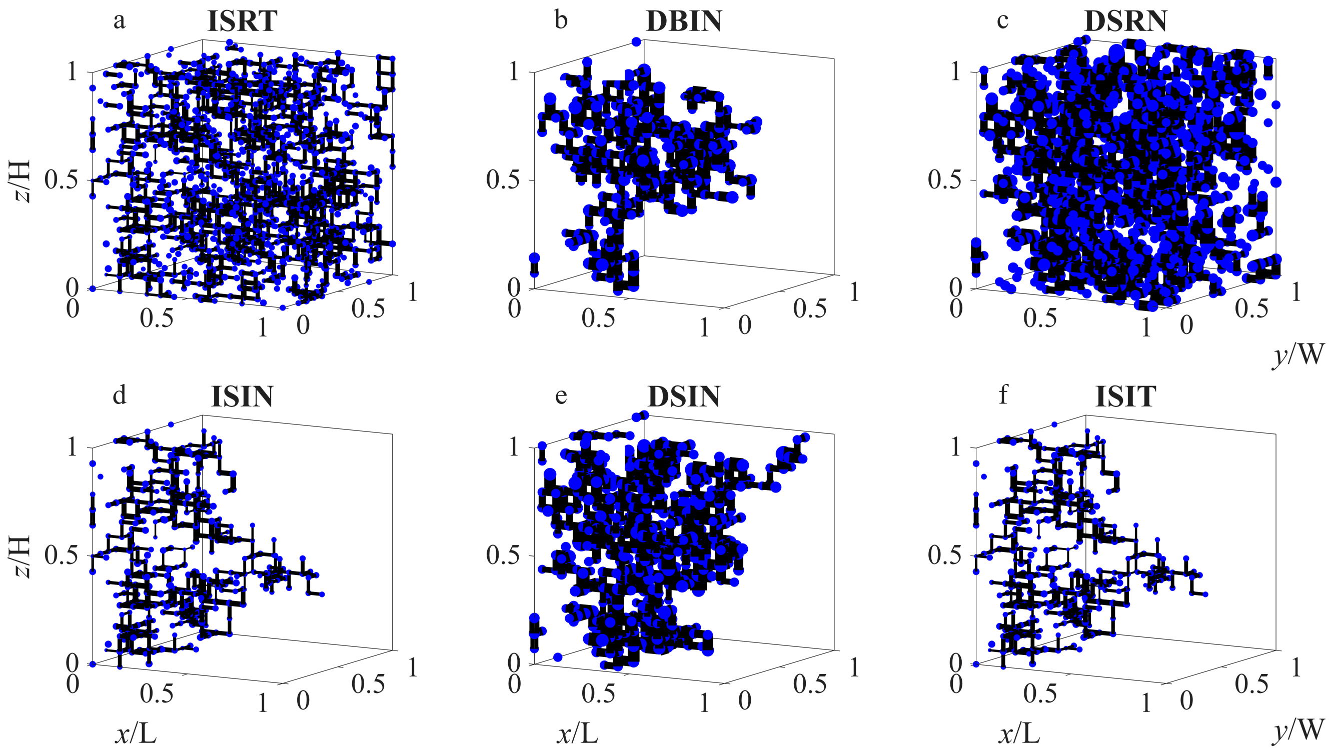

Figure 4. Pores (blue spheres) and throats (black cylinders) filled with the invading phase at breakthrough (sample spanning percolation) for the different displacement modes. The plotted cases are the simple-cubic lattice realization "r_2", for the $N = 15$, medium PSD variability ($CV = 0.5$) with correlation between the pores' and throats' size.

2.3 Limitations

2.3.1 Scope

In this manuscript, we address the quasi-static (i.e., negligible viscous forces) displacement of two immiscible, incompressible fluids, without background pressure gradients, i.e., negligible inertial and gravitational forces, and without variability in the surface tensions or wettability. Moreover, the domain is assumed rigid (undeformable), and the pore bodies (sites) have no spatial correlation.

Dynamic effects on the displacement processes and hysteresis are relevant to most multiphase flow problems. In this, the number of simultaneously invaded pores (Onody et al., 1995), the dynamic breakup and snap-off of NWP ganglia (Dias and Payatakes, 1986), trapping of the WP (when neglecting film flow)(Chandler et al., 1982), and many more phenomena affect the phase configuration and hysteresis in the saturation and permeability curves (Piri and Blunt, 2004, 2005a, b). Despite its significance, the effect of the flow hydrodynamics on hysteresis is not in the scope of this manuscript but will be in a future analysis.

https://doi.org/10.5194/egusphere-2026-4185
Preprint. Discussion started: 27 July 2026

Here, we use a contact angle of 30° to describe the wettability of the wetting phase. However, the importance and physical interpretation of this value are limited by the mentioned complexity of the pore shape (within the simplified, quasi-static displacement simulated here, the capillary head for other contact angles (θ) simply scale with cosine (θ)). The variability in the advancing and receding contact angle is commonly related to viscous forces; thus, in our quasi-static case, its disregard is justified. The effect of hysteresis in the contact angle on the retention and permeability curves is discussed in several works (Braun and Holland, 1995; Friedman, 1999; Zhou, 2013; Fu et al., 2021).

Disregarding the gravitational forces is justified for low *Bond numbers* $Bo = \frac{\Delta \rho g d^2}{\sigma}$. If we assume that $d = 2r_\mathrm{s} = 0.01$ cm, and address water and air fluids ($\Delta\rho = 1$ g/cm^3), then $Bo \approx 1.3 \cdot 10^{-3}$, that is, the capillary forces are much more significant than the gravitational ones. The interesting effect of gravity on hysteresis is discussed in other works (e.g., Heinse et al. (2009)).

The effect of fluid compressibility is expected to be negligible in the (many pores) microscale (Hunt and Sahimi, 2017). According to the ideal gas law, the density of gases is proportional to their pressure. Thus, the gas volume difference is proportional to its pressure difference, which is very small in quasi-static (no) flow conditions and no gravity forces. In any case, the main effect of compressibility is to reduce the trapping of the non-wetting phase (Larson et al., 1981a), which is bounded by the no-trapping scenarios.

2.3.2 Lattice size

Generally, a small domain may cause ill-representation, such as obtaining sample-spanning percolation that differs from the theoretical (of infinite lattices) percolation thresholds, that is, the fraction of sites occupied by the invading phase (p_cs) when a sample-spanning (connecting inlet and outlet faces) percolation is obtained. In turn, this may cause a significant error, for example, in the estimation of the expected network permeability, especially for saturation degrees near the percolation threshold (Wilkinson, 1986). Diaz et al. (1987), Chatzis and Dullien (1982), and Yu et al. (1986) respectively, report that networks of $15 \times 15 \times 15$, $18 \times 18 \times 12$, and $20 \times 20 \times 20$ pore-bodies are required to give satisfactory results. The lattice size used in this work ($15 \times 15 \times 15$) is similar to that used by others, e.g., Diaz et al. (1987). Jerauld and Salter (1990) reported only little differences between cubic networks with $16 \times 16 \times 16$ and $32 \times 32 \times 32$.

Here, we use three realizations for each lattice, in order to mitigate some of the effects of the finite lattice size. The variability between the different realizations (in the retention and permeability curves) is an indication of the bias of the limited lattice on the assumption of the continuous radii distributions, and small sample statistics. Comparing the mean values (of saturation and permeability) between realizations of different scenarios allows a good distinction of the main (considered) effects from the size bias effect. In addition, Appendix A presents a sensitivity analysis of the effects of the finite lattice size on the different aspects evaluated in this work. Namely, the effect of the lattice size on the intrinsic permeability is evaluated in Figure A1 in the Appendix. Moreover, comparing the retention and permeability curves of the two main scenarios (ISRT and DBIN) for a $N = 20$ (Figure A3 in the appendix) shows that the lattice size affects the trapping (more trapping in the larger lattice) and slightly affects the sensitivity (differences between realizations), but does not affect the conclusions in this work. The DBIN retention curves on a $N = 20$ (orange) and $N = 15$ (red) are similar except for the breakthrough (Δ), that is, the arrival of the invading phase at the opposite (from the inlet) lattice face. This is supported by the statistics of the percolation thresholds. In this,

https://doi.org/10.5194/egusphere-2026-4185
Preprint. Discussion started: 27 July 2026

p_{cs} the sites occupation at breakthrough, is not affected by the lattice size for the RP cases (ISRT) and slightly (insignificantly) decreases in the IP scenarios (DBIN, Fig. A5). Moreover, the percolation thresholds determined in this work are similar to the previously determined values (Hunt and Sahimi, 2017; Kurzawski and Malarz, 2012; Wang et al., 2013; Wilkinson and Willemsen, 1983), further supporting the applicability of the $N = 15$ lattice. Namely, in the context of permeability curves, the finite $N = 15$ lattices size provides the correct percolation thresholds, and the finite size effects are expected to be small far away from the percolation thresholds. Thus, it can be safely concluded that this effect is small throughout the whole range of saturation degrees. The effect of periodic vs confined boundaries were also evaluated in a sensitivity analysis. Interestingly, the periodic domain did not reduce (and even increased) the variability of the permeability (shaded regions in Fig. A1a) or the coefficient of variation (Fig. A1b), thus, we did not use the periodic condition in our analysis.

2.3.3 Pore geometry and phases occupancy

The simplified pore geometry applied in this work, namely the cylindrical bonds and spherical bodies, and the assumption that each element (bond or site) is filled with a single phase, may not be accurate in describing porous media, especially coarse-texture materials. The single-phase occupation was employed for only the phase volume evaluation, but the conceived W-phase films (of assumed negligible volume) allow (justify) imbibition by a RP process and their non-trapping feature. These assumptions are controversial in dynamic flow simulations as they misrepresent important displacement mechanisms such as (capillary, surface tension-induced) snap-off and (viscosity-induced) dynamic breakup (Joekar-Niasar et al., 2010). However, in the case of quasi-static conditions, these simplifications are justified. Other contributions evaluated the different effects of different media properties, such as the grains (glass beads) size distribution (Laroussi and De Backer, 1979); the ratio between bond and site radii (Assouline and Rouault, 1997; Jerauld and Salter, 1990); the effect of angular pores (Diamantopoulos and Durner, 2015); and the effect of unconsolidated media (Naar et al., 1962).

2.3.4 Singularities

In this work, a minimal value (of ten orders of magnitude smaller than the sum of each site bonds' conductances) is added to the non-conducting bonds before inverting the matrix to evaluate the pressure distribution and the permeability. This practice is used to avoid singularity in the Laplace matrix resulting from an isolated phase that is not connected to the inlet or outlet. This practice is simpler and faster compared to alternatives such as applying search and elimination algorithms (Raoof and Hassanizadeh, 2010) or even applying the singular value decomposition (SVD) pseudo-inverse approximation (Ben-Noah et al., 2024b). The effect of this addition was evaluated by comparing the calculated relative permeability values at different saturation degrees to those obtained by using SVD, and it was found to be completely negligible (not presented).

3 Results and Discussion

In this section, the results of the simulations for the different displacement modes (Table 1) are presented and discussed. First, the different hysteresis mechanisms, as reflected in the different simulations, are discussed from both retention and relative

https://doi.org/10.5194/egusphere-2026-4185
Preprint. Discussion started: 27 July 2026

permeability standpoints. Next, the effects of: the spread of the pore size distribution (section 3.2), correlation between pore bodies' and throats' (3.3), and pore system connectivity (3.4) are analyzed with respect to hysteresis in the retention and relative permeability curves. Finally, a short correspondence to the p_w and p_d functions of hysteresis models is presented (3.5).

3.1 Different hysteresis mechanisms

3.1.1 Retention curve

Combined effects:
The combined effects of the different hysteresis mechanisms manifest in the main curves of the Imbibition Site-Random percolation with Trapping of the NWP (ISRT, blue) and the Drainage Bond-Invasion percolation with No trapping of the WP (DBIN, red), depicted in Figures 5a and c. The I/DSRN (purple line) represents the "ideal" reversible (non-hysteretic) filling order of pores by their size, i.e., smallest to largest in imbibition (ISRN) and the other way round during drainage (DSRN).

The similarity between the 3 realizations (different line types in Fig. 5 top panels and shaded regions in the bottom panels) suggests that 3 realizations are sufficient to be representative of the continuous $f(r)$ distributions, and of the various displacement mechanisms. The "air entry" value, the h_c value in which S_w is still 1, of DBIN ($\approx 10\ cmH_2O$) is slightly larger than that of I/DSRN ($\approx 6\ cmH_2O$), Fig. 5c, suggesting that the widest pore throat at the inlet face, which is drained first during DBIN, is smaller than the size of the biggest pore body in the entire domain, which imbibes last (drains first) in I/DSRN (remembering that "ISRN" differs from "DSRN" only in the direction). The small difference between the air entry values is due to the reciprocal relation between the capillary head and the curvature radius, following Young-Laplace equation, and the pore system under consideration corresponding to relativity coarse-textured media. Following the same reasoning, the full drainage capillary head value (the largest h_c value where $S_\mathrm{w} \to 0$, corresponding to the smallest pore) of DBIN, is larger than that of I/DSRN. This may also be explained through the Ink bottle hysteresis, that is, by the difference between bond-controlled and site-controlled displacements. This is supported by the similarity between ISRT and I/DSRN at the high h_c values. The effect of trapping is notable as the ISRT (blue) diverges from the ISRN (purple) at a WP saturation degree value of $S_\mathrm{w} \approx 0.2$ and attains its maximum saturation of $S_\mathrm{w} \approx 0.5$. The disconnection of the NWP ("∇" for ISRT and ISRN) occurs at a similar $S_\mathrm{w} \approx 0.2$ as the divergence of the curves. As expected, in the "ideal" RP without trapping (I/DSRN) case, the breakthrough ("Δ") of one phase is the same as the disconnection ("∇") of the other phase. The theoretical values of the occupation probability (number fraction of sites occupied by a phase) for simple-cubic random site percolation (at the breakthrough) is $p_\mathrm{cs} \approx 0.3115$ (Wang et al., 2013). The slightly higher I/DSRN p_cs value obtained here (0.333 ± 0.019) is explained by the small number of realizations (3) compared to the high variability due to the finite lattice size (Fig. A5).

Trapping:
Comparing the imbibition retention curve of site-random percolation with (ISRT, blue) and without (I/DSRN, purple) trapping (Fig. 5c) and also the site-invasion percolation with (ISIT, green) and without (ISIN, navy-blue) trapping (Figure 5d), it can be seen, as expected, that the trapping affects the hysteresis only at low h_c values, while in the dryer section (high h_c), the curves are similar. Also, the S_w and h_c related to the sample spanning percolation (cluster) of the invading phase (marked with Δ)

https://doi.org/10.5194/egusphere-2026-4185
Preprint. Discussion started: 27 July 2026

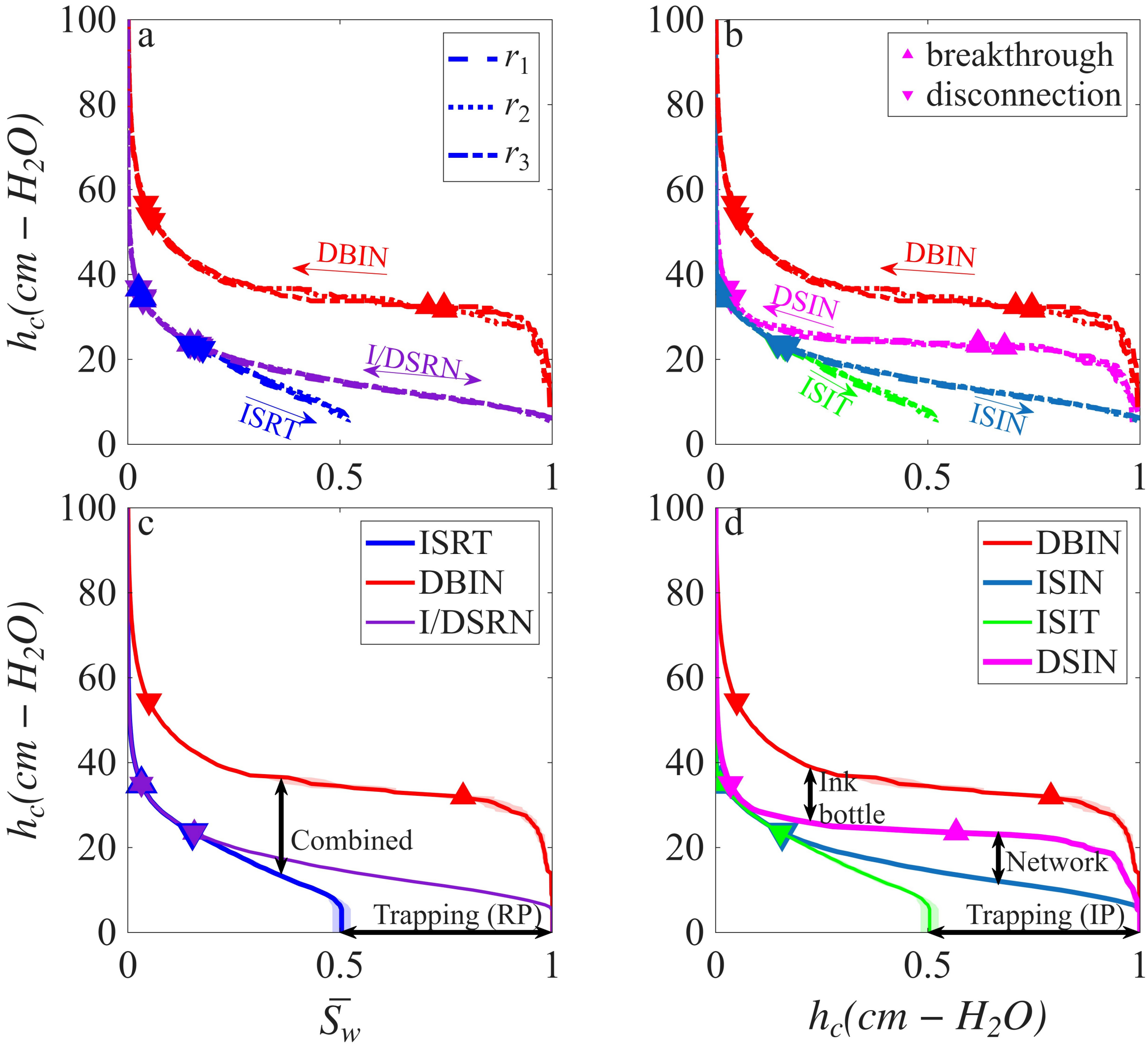

Figure 5. Retention curves of the three realizations (top panels, r_1 to r_3) and the mean curves (bottom panels) for: imbibition site-random-percolation with trapping of the NWP (ISRT, blue, panels a and c), drainage bond-invasion-percolation without trapping of the WP (DBIN, red, all panels), the reversible site random percolation without trapping (I/DSRT, purple, panels a and c), imbibition site invasion percolation with (ISIT, green, panels b and d) and without (ISIN, navy-blue, panels b and d), drainage site invasion percolation without trapping of the residing WP (DSIN, magenta, panels b and d) and with trapping of the residing NWP. The breakthrough of the invading phase (formation of a sample-spanning cluster) is marked with upward pointing triangles (Δ), while the disconnection of the residing phase is marked with downward pointing triangles (∇). The pore size distributions (PSD) of these realizations are given in Fig. 1b and d ($CV = 0.5$).

are the same for the scenarios with and without trapping, suggesting that below the percolation threshold the trapping of the resident phase is negligible. The similar effect of trapping on the different percolation modes, that is, invasion (ISIT vs ISIN)

https://doi.org/10.5194/egusphere-2026-4185
Preprint. Discussion started: 27 July 2026

and random (ISRT vs ISRN), can be explained by the well-connected simple-cubic lattice with a coordination number of $N_\mathrm{c} = 6$. Interestingly, the S_w and h_c at the disconnection point of the residing (NW) phase (marked with ∇) are similar for the imbibition cases, with and without trapping. This suggests that most of the NWP trapping occurs at WP occupation probabilities higher than the disconnecting threshold.

Ink-bottle hysteresis:

In contrast to the effect of trapping being limited to high S_w and low h_c, the effect of the bond (DBIN, red) vs site (DSIN, magenta) displacement (Fig. 5d) is visible in the entire span of h_c values, i.e., for any h_c value, S_w of DBIN is larger than that of DSIN. However, despite the similar S-shaped curves, this effect is not uniform, where the differences in h_c are slightly larger in low S_w than near W-saturation. The S_w at the sample-spanning percolation of the invading NWP ("breakthrough") of DSIN (magenta Δ) is slightly smaller than that of DBIN (red Δ), suggesting that site-controlled invasion displaces larger pores at lower occupation probability than bond-controlled invasion, despite the correlation between r_s of adjacent pore bodies and r_b of their connecting pore throats. This is also supported by the lower S_w at the disconnection of the residing WP (∇) of DSIN compared to DBIN. This is because the bond radius (r_b) is correlated to the geometrical mean of r_s, thus, the bond displacement does not necessarily drain the sites from largest to smallest r_s.

Network hysteresis:

As discussed above in the Theory section (1.1), network hysteresis is explained by IP, in which surrounding pores defend a central pore from being invaded. In this respect, the direct difference between IP and RP is negligible, as seen by comparing ISRT (blue) with ISIT (green) and I/DSRN (purple) with ISIN (navy-blue) in Fig. 5. This also suggests that the effect of the finite-size domain is not significant. The similarity between the IP's and RP's h_c and S_w corresponding to the disconnection of the residing NWP (∇), is surprising because the site-percolation threshold of RP ($p_textrmcs \approx 0.311$, Wang et al. (2013)) is expected to be larger than for IP (≈ 0.16 for $N = 15$, Wilkinson and Willemsen (1983)), that is, the number of sites imbibed at the breakthrough is larger for RP (Fig. 4). The similarity can be explained by the log-normal distribution of pore sizes, resulting in many small pores which do not affect the S_w at breakthrough. For illustration, at the breakthrough, the mean $\bar{S_\mathrm{w}}$ of ISIT is 0.01, and that of ISRT is 0.03, which is in accordance with the ratio between the two p_cs. Interestingly, at breakthrough, the $\bar{h_\mathrm{c}}$ of ISIT is equal to that of ISRT ($\approx 35\ cm - H_2O$). This suggests that the invasion percolation path has a similar maximum pore size connecting the sample-spanning cluster as the critical pore size of a random percolation process. This insight supports the applicability of the critical path analysis (Ambegaokar et al., 1971; Friedman and Seaton, 1998) for IP and RP. The occupation probability of the NWP during imbibition at the disconnection point of the IP (ISIT and ISIN) is $\approx 0.345 \pm 0.01$, which is similar to the p_cs of the RP cases (ISRT and I/DSRN) ($\approx 0.344 \pm 0.01$). This value is close to the theoretical value of the random site-percolation threshold for a simple-cubic array (0.311), and far from the value expected for the invasion percolation threshold(ca. 0.16). The similarity in the occupation probability of the NWP at disconnection for RP and IP during imbibition is not trivial, suggesting that the expulsion of the residing NWP near disconnection is akin to RP rather than to IP.

Moreover, the combined effects of the filling order and invasion percolation (network hysteresis) can be analyzed by the difference between the drainage (DSIN, magenta) and imbibition (ISIN, navy-blue) site-invasion percolation (without trapping) (Fig. 5d), and between the drainage site random (I/DSRN, Fig. 5c) and invasion (DSIN, Fig. 5d) percolation (without trapping).

https://doi.org/10.5194/egusphere-2026-4185
Preprint. Discussion started: 27 July 2026

These analyses show that the network hysteresis affects the retention curve shape and the width of the hysteretic loop. In this, while the capillary head (h_c) at the WP saturation ($S_w = 1$) is the same for both DSIN and ISIN (akin to the largest pore), the S_w under ISIN increases almost linearly with the decrease of h_c, and DSIN presents an S-shaped curve. Also, as expected, the S_w of the drainage is larger than that of the imbibition curve for any value of h_c. This is because h_c during drainage, at each step, attains the largest value (related to the smallest drained pore) while during imbibition, the h_c value corresponds to the largest pore (of lowest h_c). These differences suggest that the filling order of the pores during imbibition is not a mirror image of the drainage order, and network hysteresis is significant even for $3D$ networks with a coordination number of 6. In addition, the saturation degree related to the sample-spanning cluster (marked with Δ) formed in imbibition is much smaller than that of drainage. This is to be expected because of the pore-filling order, where the volume of the same fraction of occupied sites (p_{cs}) is larger when they are taken from the largest to the smallest than the other way round. The decoupled effect of the pore filling order can be evaluated by the difference between the breakthrough and disconnection points in the reversible I/DSRN case. In such a comparison, the breakthrough during DSRN (purple Δ in Fig. 5c) is obtained at a similar h_c as that of the DSIN (magenta Δ in Fig. 5d), but at much smaller S_w, which is due to the network hysteresis.

3.1.2 Permeability curves

Combined effects:

The relative permeability curves of the different scenarios are presented in Figure 6. The relative permeability of the W-phase (k_r^W) during drainage (DBIN, red solid line, Fig. 6a) is unity until h_c attains the "air entry" (NW) value, related to the largest pore throat, which is larger than the "air entry" value of the "ideal" curve (I/DSRN, porpule), related to the largest pore body in the domain. The "air entry" pressure value for imbibition through RP (ISRT, blue) is the same as the "ideal" value. The maximum k_r of the W-phase during RP imbibition (ISRT) is significantly smaller than unity (approximately 0.25) due to the presence of a trapped NWP. Similar values have been reported, for example, in imbibition of Berea sandstone (Piri and Blunt, 2005a). The trapped NWP occupation probability at the end of the ISRT simulation (maximum k_r^w) is 0.173 ± 0.003. The dramatic effect of this fraction on the S_w (Fig. 5a) and k_r^w (Fig. 6a) is because of the filling order (from small to larger pores) and the correlation between the site and bond radii, so that the potential contribution of the large pores (with trapped NWP) are more significant to the conductance of the lattice. The h_c values at which the ISRT k_r^W (solid blue line, Fig. 6a) and the DBIN k_r^{NW} (red dashed line) intersect with the x-axis correspond to the sample-spanning percolation values (Δ in Fig. 5), while the ISRT k_r^{NW} and DBIN k_r^W reach zero at the disconnection points values (∇ in Fig. 5). The $k_r^{NW}(h_c)$ curves are concave (of negative curvature), which can be explained by the filling order and correlation between the pore bodies' and throats' radii, so that the larger pores affect the relative permeability more than small pores. This shape can be well represented by an exponential function ($k_r^{NW} = 1 - exp(-\alpha h_c)$, Ben Noah and Friedman (2015)). The network's sample-spanning connectivity of the NW-phase for the ISRT breaks down at lower h_c values than the breakthrough for DBIN. Moreover, the slope at which the k_r^{NW} rises with h_c is larger for ISRT than for DBIN. This means that far from the disconnection point, RP imbibition (ISRT) only slightly reduces k_r^{NW}, while near disconnection the effect is very sharp. This effect is even more notable in the $k_r^{NW}(S_w)$ curve (Fig. 6c), with a sharp drop from k_r^{NW} of about 0.75 to 0.

https://doi.org/10.5194/egusphere-2026-4185
Preprint. Discussion started: 27 July 2026

Similarly, the networks are permeable to the W-phase at a larger h_c for DBIN than for ISRT. However, this difference in the W-phase permeability threshold is not visible in terms of S_w (Fig. 6c). The permeability is considered less hysteretic in the S_w compared to the h_c (Assouline and Or, 2013; Mualem, 1986). This is partially supported by the results presented in Fig. 6c compared to Fig. 6a. The $k_\mathrm{r}^{NW}(S_\mathrm{w})$ hysteretic loop between DBIN and ISRT (Fig. 6c) is non-monotonic, i.e., the imbibition (ISRT, blue) k_r^{NW} of low S_w is higher than the DBIN k_r^{NW}. However, when S_w increases the ISRT k_r^{NW} drops quickly below the DBIN k_r^{NW}. Conversely, the k_r^{W} of DBIN is higher than that of ISRT for all the S_w range. Compared to the reversible I/DSRN, DBIN k_r^{W} is higher at low S_w and similar at high S_w. Interestingly, the k_r^{W} vs S_w curves (solid lines in Fig. 6c) of the different processes have different curvatures. In this, the k_r^{W} curves of ISRT (blue), I/DSRN (purple), ISIT (green), and ISIN (navy-blue) are of mainly positive curvature (until approaching their maximum values), suggesting that the early imbibed pores (after breakthrough) have a smaller effect on k_r^{W} than the larger pores, which are filled lastly (during imbibition). In contrast, in drainage, DBIN (red) and DSIN (magenta), presents quite a negative curvature at low S_w, similar in magnitude to the positive curvature of the imbibition curves. At high S_ws, the nearly linear relation suggests that the effect of the pores' draining order (from larger to smaller) on the saturation is comparable to its effect on the permeability. Also interesting is the more significant variability between realizations (colored regions) in the $k_\mathrm{r}(S_\mathrm{w})$ compared to the $k_\mathrm{r}(h_\mathrm{c})$ curves and for the drainage cases DBIN (red) and DSIN (magenta), compared to the imbibition ones.

Trapping:

Similarly to the retention discussed above, the effect of trapping, comparing ISRT with I/DSRN (Fig. 6a) and ISIT with ISIN (Figure 6b), is visible only at the low h_c values, and only for the k_r^{W}, because the trapping occurs mostly after the disconnecting of the NWP, i.e., where $k_\mathrm{r}^{NW} = 0$. The k_r^{NW} curves of ISRT and I/DSRN, and ISIT and ISIN overlap, thus are invisible in the charts. Moreover, the effect of trapping is similar for the IP (ISIT and ISIN) and RP (ISRT and DSRN) cases, and also in both $k_\mathrm{r}(h_\mathrm{c})$ (top panels of Fig. 6) and $k_\mathrm{r}(S_\mathrm{w})$ (bottom panels) curves.

Ink-bottle hysteresis:

Comparing drainage invasion-percolation governed by the bonds (DBIN) to that governed by the sites (DSIN) (Figure 6b) shows resemblance in the shape of the curves, with a right shift towards higher h_c in the DBIN compared to the DSIN. The ink-bottle hysteresis, given by the difference between DBIN and DSIN, is more notable in the $k_\mathrm{r}(h_\mathrm{c})$ curves (Figure 6b) than in the $k_\mathrm{r}(S_\mathrm{w})$ curves (Figure 6d). It is also visible that the variance between realizations is larger in the DBIN case. This is to be expected because the bond radius (r_b), determining the invasion order, and the site radius (r_s), determining its volume, are not directly correlated but rather correlated through the geometrical mean of adjacent r_s.

Network hysteresis:

The relative permeability curves, $k_\mathrm{r}^{W}(h_\mathrm{c})$ and $k_\mathrm{r}^{NW}(h_\mathrm{c})$, of the invasion percolation (ISIT, green lines, Figure 6b) are very similar to the random percolation (ISRT, blue lines, Figure 6a). The network hysteresis is revealed by comparing the drainage (DSIN, magenta) and imbibition (ISIN, navy-blue) site-governed displacement through invasion percolation (Figure 6b). The $k_\mathrm{r}^{W}(h_\mathrm{c})$ of the drainage (DSIN) is larger than that of imbibition (ISIN) to all h_c values, with a uniform shift except at the ends ($k_\mathrm{r}^{W} \to 0$ and $k_\mathrm{r}^{W} \to 1$), where the shift is smaller. Conversely, the $k_\mathrm{r}^{NW}(h_\mathrm{c})$ curves originate from the same h_c (disconnection of the NWP for ISIN and breakthrough of the NWP for DSIN) and diverge with increasing h_c where ISIN k_r^{NW} increases more

https://doi.org/10.5194/egusphere-2026-4185
Preprint. Discussion started: 27 July 2026

steeply. Notice that ISIN k_{r}^{NW} equals that of ISIT (green). For $k_{\mathrm{r}}^{W}(S_{\mathrm{w}})$ curves, DSIN and ISIN present a closed hysteretic loop in the lower half of the saturation degree. The $k_{\mathrm{r}}^{NW}(S_{\mathrm{w}})$ curves present a crossover behavior where ISIN k_{r}^{NW} is larger than that of DSIN in low S_{w}, but reaches the disconnection point (sharp drop to zero) at a much lower S_{w} than the breakthrough point of DSIN. The similarity between DBIN and DSIN (Fig. 6d) suggests that the ink-bottle mechanism does not significantly affect either the WP or NWP curves. Correspondingly, the similarity between ISIT and ISRT, or ISIN and I/DSRN, suggests that the percolation mode (IP vs RP) does not affect the hysteresis of the $k_{\mathrm{r}}(S_{\mathrm{w}})$ curves. This means that network hysteresis is responsible for the hysteresis of $k_{\mathrm{r}}(S_{\mathrm{w}})$ at low S_{w}, and that trapping is the main hysteretic mechanism for high S_{w}.

3.2 Effect of variation in the pore size distribution

3.2.1 Retention curve

Combined effects:
Figure 7 presents the effect of the variation in the pore size distribution (PSD, Fig. 1) on the different scenarios. Increasing PSD coefficient of variation increase the difference between the retention curves evaluated in the 3 realizations. In addition, the PSD variation affects the invading-phase breakthrough, the residing-phase disconnection point, and the shape of the retention curves. The low variation cases, with $CV \equiv \frac{\sigma_k}{\mu_k} = 0.2$, Fig. 7a and b, are less sensitive to the different realizations compared to the medium variation ($CV = 0.5$, Fig. 5) and high variation ($CV = 1$, Fig. 7c and d). The differences between realizations in the high-variation cases are more notable in the drainage DBIN and DSIN (red and magenta shaded regions) than in the imbibition (ISRT, ISIT, ISIN, and also the I/DSRN) curves.

In the ISRT (blue) process, increasing the variation of the PSD increases the breakthrough (Δ) h_{c} and decreases its S_{w}. This is because the critical pore size (corresponding to the percolation threshold, $p_{\mathrm{cs}} \approx 0.3115$), of higher h_{c}, decreases with increasing variation in PSD. On the other hand, the disconnection of the NWP during ISRT is at a similar h_{c} and in a much lower S_{w}, suggesting that the critical pore of disconnection is less affected by PSD-variation, but the phase volume does. Or in other words, in the high CV case, a significant part of the saturation is in a few very large pores, which are being invaded lastly (if at all). This observation can also explain the larger fraction of entrapped air in the high-CV case (maximum $S_{\mathrm{w}} \approx 0.35$) compared to the low CV (maximum $S_{\mathrm{w}} \approx 0.7$). This suggests that imbibition via the quasi-static, strictly capillary equilibrium mechanism is expected to trap a significant fraction of the NWP, which means that experiments in water/air systems, with typically smaller fraction of trapped air (Topp, 1969; Mualem, 1973), are affected by dynamic process related to the viscosity ratio of the phases. In addition, the simplified geometry and processes accounted by the pore-network assumes that a pore is either WP-filled or NWP-filled, causing an over-estimation of the trapped NWP volume, while in reality, both phases can co-exist in a single pore through thick films (especially in coarse media). This effect is magnified by the air compressibility. On the other hand, this ill representation of real media affects the saturation degree but not the effective saturation (of the connected WP) and its permeability.

Increasing the PSD-variation decreases the breakthrough (Δ) h_{c} and S_{w} of the DBIN case, and increases the disconnection (∇) h_{c} but reduces its S_{w}. In consequence, the PSD-variation has a dual effect on the combined hysteresis (ISRT vs DBIN): On one hand, the retention curves shift to the left with increasing CV, which narrows the hysteretic loop. On the other hand, a higher

https://doi.org/10.5194/egusphere-2026-4185
Preprint. Discussion started: 27 July 2026

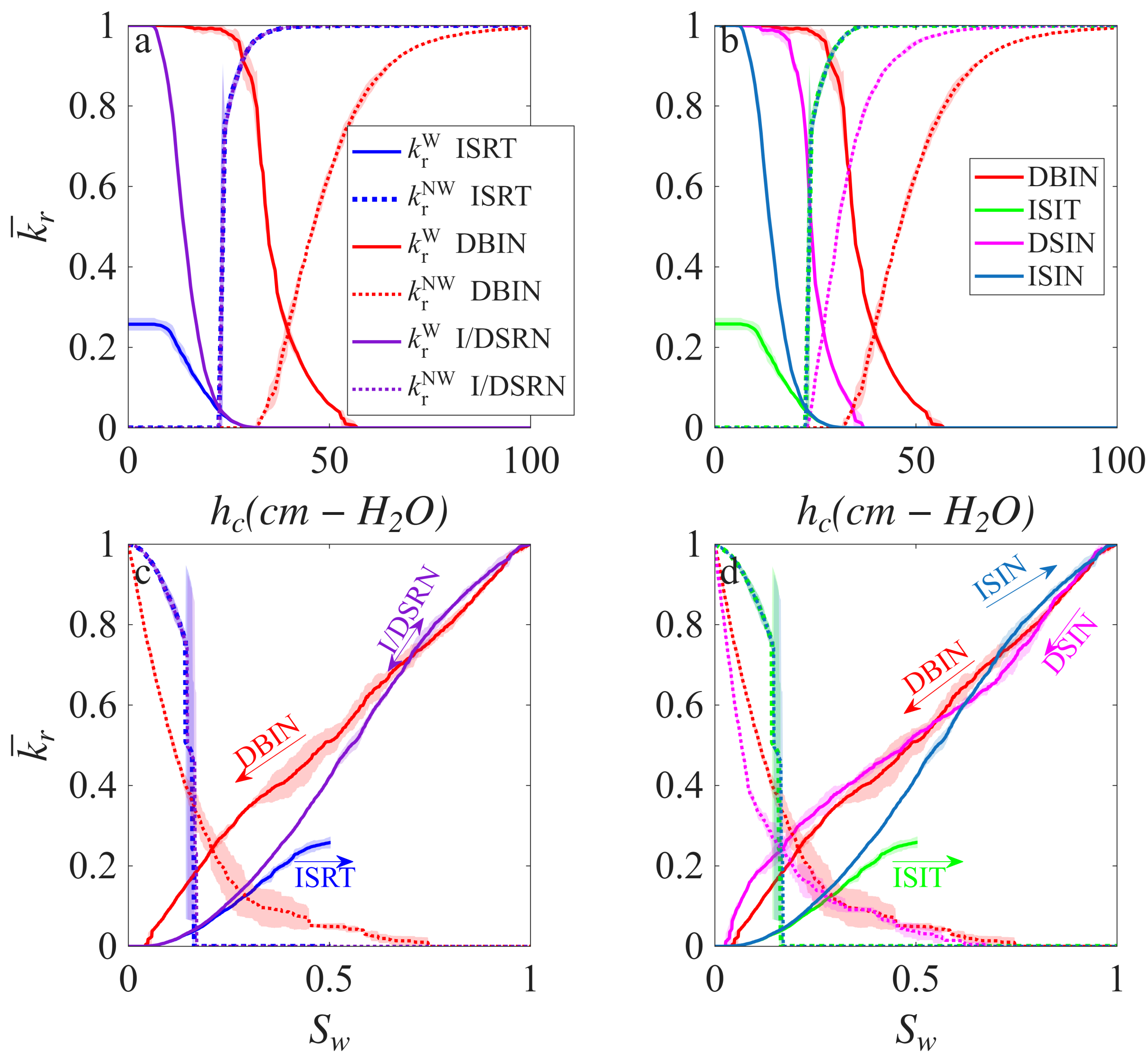

Figure 6. Relative permeability curves of the WP (solid lines) and the NWP (dotted lines), depending on the capillary head (h_c, top panels) and WP saturation degree (S_w, bottom panels) for the different displacement mechanisms indicated in the legends.

CV results in a smaller maximum S_w in the ISRT process, hence widening the hysteretic loop. The hysteretic curves' shapes are also different, where at low CV the curves have a plateau at low h_c values (related to the larger "air entry" value), while the high CV curves present a sharp decline in S_w from the minimum h_c (small "air entry" value).

Trapping:

The combined effect of the PSD-variation and the trapping mechanism can be evaluated by comparing the ISRT (blue lines) and the I/DSRN (purple lines) in Figs. 7a and c, and the ISIT (green lines) and the ISIN (magenta lines) in Figs. 7b and d. Increasing

https://doi.org/10.5194/egusphere-2026-4185
Preprint. Discussion started: 27 July 2026

the CV increases the volume of the entrapped resident phase. In this, both trapping and no-trapping cases have similar invading phase breakthrough and residing phase disconnection values, and similar retention curve shapes. However, there is a notable difference in the amount of trapped NWP and in the span of S_w values in which the trapping affects the retention, thus in the high CV, the trapping occurs at a lower S_w value. This can be explained by the higher fraction of volume assigned to a smaller number of pores in the highly variable PSD, the same fraction of trapped pores results in a much higher NWP volume.

Ink-bottle hysteresis:

Comparing the DSIN (magenta lines in Fig.7b and d) with the DBIN (red lines) reveals that the ink-bottle hysteresis loop narrows with an increase in PSD-variation. At the same time, the effect of CV on DSIN is very small compared to the effect of the variation on DBIN. This is probably due to the larger fraction of small r_b in the $CV = 0.2$ case (Fig. 1d) compared to that of $CV = 1$ (Fig. 1f). In other words, increasing PSD-variation brings the r_b and r_s distributions closer. Thus, it mitigates the bottle ink hysteresis mechanism.

Network hysteresis:

The combined effect of PSD-variation and the different percolation mode is estimated by comparing the differences between ISIT (green lines, 7b and d) and ISRT (blue lines in Fig. 7a and c). It can be seen that for the high CV case (bottom panels), the h_c and S_w values at the invading phase breakthrough (Δ) and at the residing phase disconnection (∇) are similar for ISRT and ISIT. In contrast, in the low CV case (top panels), the S_w at the breakthrough in the IP cases (ISIT and ISIN) is smaller than in the RP cases (ISRT, I/DSRN). Contrary to the ink bottle effect, network hysteresis increases with the PSD-variance, indicated by the low PSD-variance ISIN and DSIN cases (navy-blue and magenta lines, Fig. 7b) being very similar in their shape and values compared to the high CV cases (Fig. 7d). This is to be expected because the difference between "protecting" and "protected" pores is larger for high-variability. The ISIN case for the high CV (Fig. 7d) has a sharp slope near saturation and a monotonically positive curvature in most S_w range, while the DSIN presents a moderated slope near saturation, an S-shaped curve, and large variability among the 3 realizations (large shaded region). The high variability is caused by 1 of the 3 realizations having a very large pore body (corresponding to more than 20% of the total porosity, seen in the ”r_3” realization in Fig. 1c) located at the inlet face. This demonstrates the importance of using realizations in a quantity that depends on the variation of the PSD, and the effect of the finite lattice size discussed in the limitations section and in the appendix.

3.2.2 Permeability curves

Combined effects:

The effect of the variation in the PSD on the relative permeability curves variability is visible in Figure 8. The less NWP trapping of the low-CV ISRT case (blue line in Fig. 8a) results in much higher maximum k_r^{W} compared to the high-CV case (Fig. 8c). Moreover, in the low-CV case, the k_r^{NW} curves (dotted lines) of the ISRT (and I/DSRN) and DBIN are very similar in shape and seem to differ only by an almost constant shift to the right for the DBIN case compared to ISRT. In the high-CV cases (Fig. 8c), the hysteretic loop is narrower in the low h_c values, especially for the NWP (dotted lines), and of varying width (widening with increasing h_c). For the NWP, the h_c corresponding to the invading phase breakthrough of DBIN (intersection of the red dotted line with the x-axis) is very close to the h_c where the residing phase loses connectivity in the ISRT (blue dotted

https://doi.org/10.5194/egusphere-2026-4185
Preprint. Discussion started: 27 July 2026

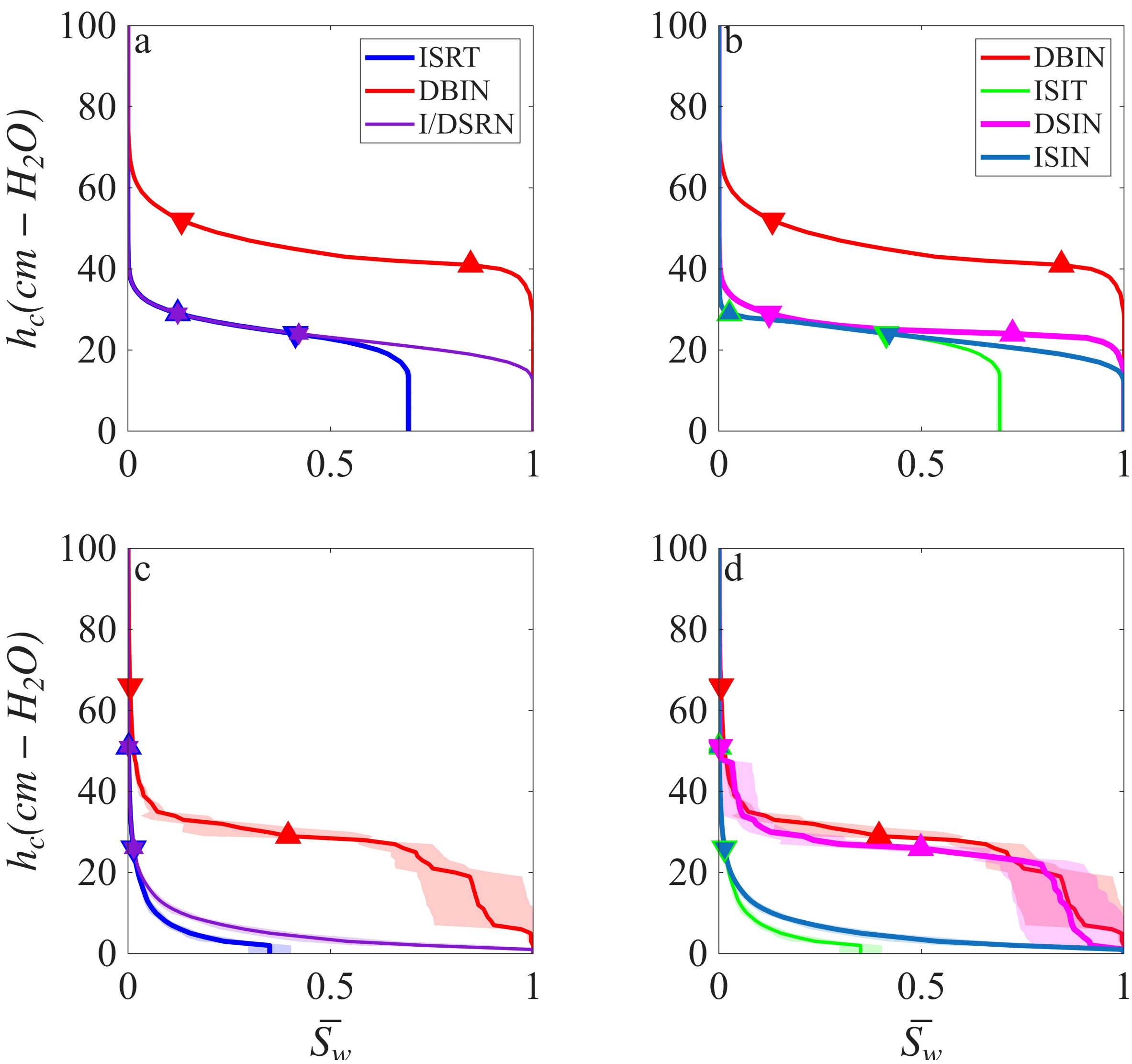

Figure 7. Retention curves for low ($CV = 0.2$, top panels) and high ($CV = 1$, bottom panels) variability in the pore size distribution for the different displacement mechanisms indicated in the legends.

line intersection with the x-axis). The intersection point of the $k_\mathrm{r}^W = k_\mathrm{r}^{NW}$ of ISRT in the high-variability case is at a very low k_r value, suggesting very little overlap in which both phases are sample-spanning continuous. In contrast, the intersection point ($k_\mathrm{r}^W = k_\mathrm{r}^{NW}$) of DBIN in the low variability is very high ($k_\mathrm{r} \approx 0.35$), keeping in mind that the intersection is limited by the sum $k_\mathrm{r}^W + k_\mathrm{r}^{NW} < 1$ (Honarpour and Mahmood, 1988). As h_c increases, the hysteretic loop widens with the DBIN k_r^{NW} increasing more moderately with h_c compared to ISRT. The DBIN (red line) $k_\mathrm{r}^W(h_\mathrm{c})$ curve of the low-CV case is almost

https://doi.org/10.5194/egusphere-2026-4185
Preprint. Discussion started: 27 July 2026

linear, except near the "air entry" value (at low h_c) and near the NWP saturation. In contrast, in the high-variability, the curve is complementary-exponential-shaped (with a left shift).

Trapping:

The combined effect of trapping and PSD-variability on the relative permeability can be evaluated by comparing k_r^W in ISRT (solid blue lines in Fig. 8) and I/DSRN (solid purple lines) or the ISIT (solid green lines) and ISIN (solid navy-blue lines). As expected, in both comparisons, the effect of trapping increases with the PSD's CV. The trapping of the NWP does not affect k_r^{NW} because even for the high-CV cases, the trapping occurs at low h_c values where the k_r^{NW} is already very low (or even zero, i.e., after disconnection).

Ink-bottle hysteresis:

Comparing the DBIN (red lines in Fig. 8) k_r curves to the DSIN (magenta lines) suggests that for both WP and NWP, the ink-bottle mechanism is more significant in low-CV PSD than in the high-CV cases. This is in agreement with the observation regarding its effect on the retention curves and the explanation provided above.

Network hysteresis:

Generally, the $k_r(h_c)$ IP (ISIT and ISIN) are very similar to the RP (ISRT and I/DSRN) processes. Comparing the DSIN and ISIN curves (Fig. 8b and d), it is clear that network hysteresis in the $k_r(h_c)$ curves (for the WP and NWP) is more significant for high-CV PSD than in the low-CV cases. Again, this is in agreement with its effect on the retention curves discussed above.

3.3 Effect of the correlation between pore bodies' and throats' radii

3.3.1 Retention curve

Combined effects:

The correlation between the pore throat (r_b) and body (r_s) radii should not affect the retention curve of the site (pore body)-governed displacement cases. This is simply because the bonds (pore throats) do not affect neither h_c nor S_w, or the pore filling order of the site-governed case. In contrast, the DBIN retention curve without PSD correlation (not presented) has a slightly higher S_w and lower h_c values at breakthrough, and a milder slope than the correlated case (Fig. 5).

3.3.2 Permeability curves

Combined effects:

In contrast to the effects (and lack of them) on the retention curve, the correlation between the pore bodies' and throats' PSDs does not affect DBIN, but does significantly affect ISRT $k_r(h_c)$ (both for WP and NWP), which is revealed by comparing the k_r curves without correlation of the PSDs (Figure 9a) to those with correlation (Fig. 6a). The correlation in the PSDs widens the combined (ISRT-DBIN) hysteretic loop of the $k_r^W(h_c)$ and narrows the hysteresis loop of the $k_r^{NW}(h_c)$ (Fig. 9a). This is mostly because the no PSD-correlation increases the maximum $k_r^W(h_c = 0)$ of ISRT, by reducing the effect of the trapped NWP on k_r^W. At the same time, the slope of $k_r^W(h_c)$ of ISRT in the non-correlated PSD (Fig. 9a) is more moderate than in the correlated case (Fig. 6a).

https://doi.org/10.5194/egusphere-2026-4185
Preprint. Discussion started: 27 July 2026

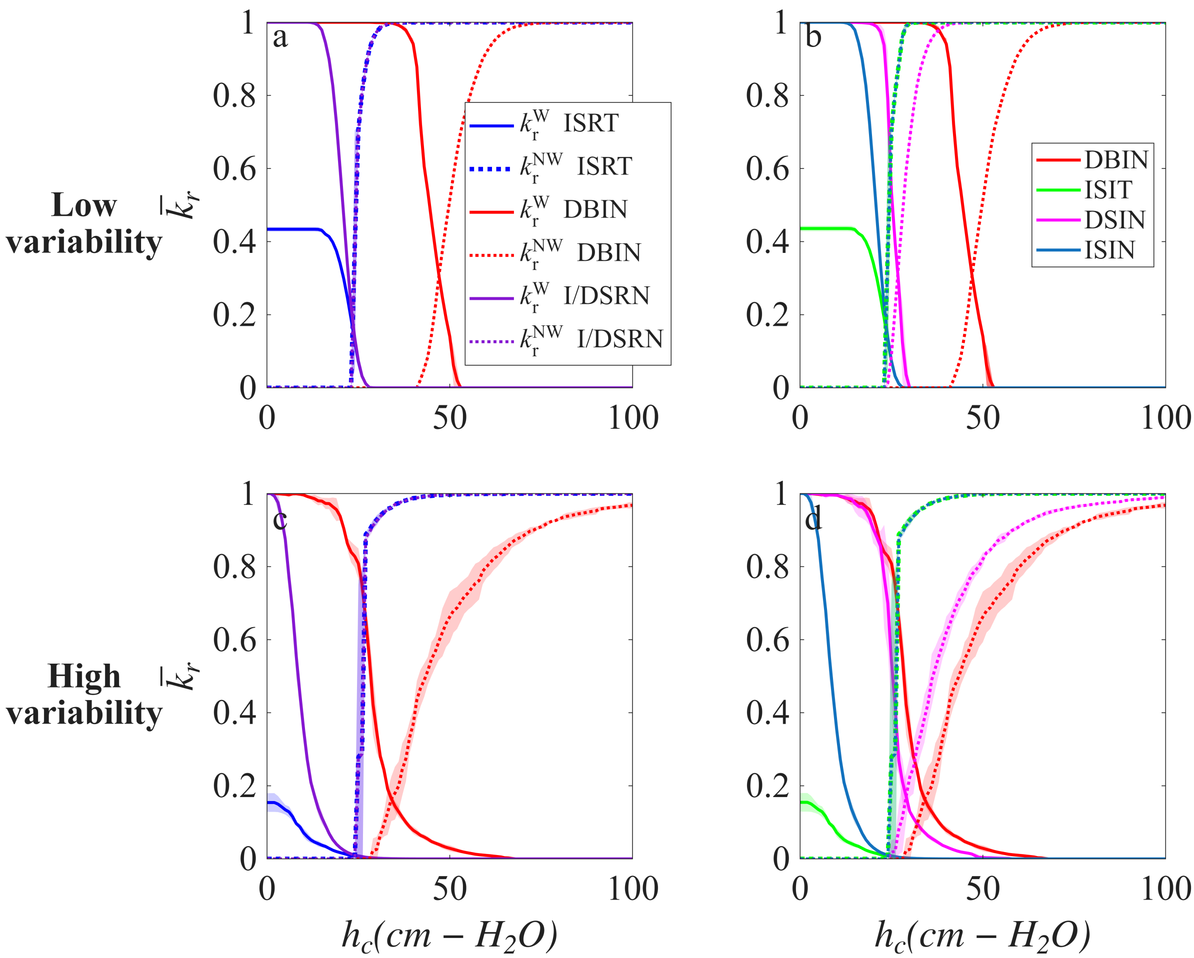

Figure 8. Relative permeability-capillary head curves ($k_r(h_c)$) of the different displacement mechanisms for the low ($CV = 0.2$, top panels) and high ($CV = 1$, bottom panels) variability in the pore bodies and throats.

Several interesting phenomena can be observed when comparing the hysteresis loops DBIN-ISRT of the $k_r(S_w)$ without correlation (Fig. 9c) to the correlated ones (Fig. 6c). First, the crossover behavior of the hysteretic loop is reversed, that is, in the correlated case discussed above (Fig. 6c) the $k_r^W(S_w)$ curves are non-intersecting with DBIN>ISRT, and the $k_r^{NW}(S_w)$ curves crossover with an intersection point near disconnection. In the no-correlation case, the opposite is observed, i.e., the $k_r^W(S_w)$ curves crossover with $k_r^W(S_w)$ of DBIN<ISRT for low S_w and the opposite for large S_w, and the $k_r^{NW}(S_w)$ curves are non-intersecting with DBIN>ISRT (Fig. 9c).

For the DBIN (red lines) case, the $k_r(S_w)$ curves (Figs. 6c and 9c) are far more affected by the correlation in the PSDs than the $k_r(h_c)$ curves (Figs. 6a and 9a). In this, the $k_r^W(S_w)$ curve reaches zero (disconnection point) at a considerably lower S_w in the correlated case compared to the uncorrelated case. At the same time, in the uncorrelated case, the k_r^{NW} curves start

https://doi.org/10.5194/egusphere-2026-4185
Preprint. Discussion started: 27 July 2026

increasing (breakthrough point) at higher S_{w} and with a milder slope compared to the correlated case. Despite that, the almost linear $k_{\mathrm{r}}^{W}(S_{\mathrm{w}})$ relationship is maintained with and without correlation. However, in the no-correlation case the slope is steeper. Conversely, the slope of the I/DSRN $k_{\mathrm{r}}^{W}(S_{\mathrm{w}})$ in the no-correlation case (Fig. 9c) is not linear (as in the correlated case) but with a negative curvature.

Trapping:

Despite the identical retention curves of the site-controlled displacement, the correlation in the PSDs increases the effect of the trapping hysteretic mechanism in both the $k_{\mathrm{r}}^{W}(h_{\mathrm{c}})$ (Fig. 9 top panels) and $k_{\mathrm{r}}^{W}(S_{\mathrm{w}})$ (Fig. 9 bottom panels) curves. The effect of trapping is similar for IP (ISIT vs ISIN) and RP (ISRT vs I/DSRN) displacement modes. The effect of the correlation on the trapping can be explained simply by the filling order during imbibition, which makes (later-filled) larger pores more likely to get trapped. For the correlated case, these pores are connected through wider throats of higher conductance. Thus, they affect the relative permeability to a greater extent. This observation partly explains the effect of the correlation on the combined hysteretic loop in the k_{r}^{W} curves.

Ink-bottle hysteresis:

The effect of the ink-bottle hysteresis (DBIN-DSIN) on the $k_{\mathrm{r}}^{W}(h_{\mathrm{c}})$ is similar with (Fig. 6b) and without (Fig. 9b) correlation between r_{s} and r_{b}. In contrast, without correlation, the $k_{\mathrm{r}}^{NW}(h_{\mathrm{c}})$ curves of DBIN and DSIN are closer then in the correlated case, and even intersecting in the high h_{c} values (Fig. 9b). This suggests that the effect of the ink bottle mechanism on the $k_{\mathrm{r}}^{NW}(h_{\mathrm{c}})$ curves hysteresis is smaller in the absence of correlation between the pore throats' and bodies' radii.

In the $k_{\mathrm{r}}(S_{\mathrm{w}})$ curves, the ink bottle dramatically affects both the WP and NWP curves. As discussed above, in the correlated case, the ink bottle effect is negligible (Fig. 6d). However, without correlation, the $k_{\mathrm{r}}^{W}(S_{\mathrm{w}})$ of DSIN is much larger than that of DBIN in the entire range of S_{w} (Fig. 9d). Compared to the linear DBIN curve, the DSIN $k_{\mathrm{r}}^{W}(S_{\mathrm{w}})$ starts at a lower breakthrough value and increases with a very steep curve (with negative curvature). In contrast, the $k_{\mathrm{r}}^{NW}(S_{\mathrm{w}})$ of DSIN, in the no-correlation case, drops sharply with the increase in S_{w} with a positive (mirroring the $k_{\mathrm{r}}^{W}(S_{\mathrm{w}})$) curvature.

Network hysteresis:

Likewise, the correlated case (Figs. 6a and b), the $k_{\mathrm{r}}(h_{\mathrm{c}})$ curves of IP and RP (e.g., ISRT and ISIT or I/DSRN and ISIN) are also similar in the uncorrelated PSDs (Fig. 9a and b). Comparing the network hysteresis (ISIN-DSIN) with (Fig. 6b) and without (Fig. 9b) correlation in the PSDs, shows that the correlation significantly narrows the $k_{\mathrm{r}}^{NW}(h_{\mathrm{c}})$ loop and slightly widens the $k_{\mathrm{r}}^{W}(h_{\mathrm{c}})$ network hysteresis loop (mainly in the low k_{r}^{W} values). Interestingly, the k_{r} value at the intersection of k_{r}^{W} and k_{r}^{NW} in the no-correlation case is the same for DSIN (magenta lines) and ISIN (navy-blue lines), while in the correlated case, the ISIN k_{r}s intersection is at a much lower k_{r} value than DSIN.

The correlation of the PSDs significantly affects the appearance of the network hysteresis effect on the $k_{\mathrm{r}}(S_{\mathrm{w}})$ curves (Figs. 6d and 9d), but does not seem to considerably affect its magnitude. In the $k_{\mathrm{r}}(S_{\mathrm{w}})$ curves without correlation, the k_{r}^{W} of both DSIN and ISIN rises more steeply with the increase of S_{w}. Thus, the largest difference between the curves occurs at a smaller S_{w} (for similar k_{r}^{W}) and at a larger k_{r}^{W} (for similar S_{w}) in the no-correlation case (Fig. 9d) compared to the correlated one (Fig. 6d). In the uncorrelated case, as in the correlated case, at large S_{w}, the effect of network hysteresis on the $k_{\mathrm{r}}^{W}(S_{\mathrm{w}})$ curves diminishes (naturally, all effects on k_{r}^{W} diminish when it approaches 1 at $S_{\mathrm{w}} = 1$). The same effect, with an opposite direction,

https://doi.org/10.5194/egusphere-2026-4185
Preprint. Discussion started: 27 July 2026

is observed in the k_r^{NW} curves, where both DSIN and ISIN curves decrease more steeply with S_w without correlation. This results in a largest difference at lower k_r^{NW} values (for similar S_w) and lower S_w (for similar k_r^{NW}), shifting the intersection of
655 DSIN and ISIN k_r^{NW}s to a lower k_r^{NW} value (Fig. 9d).

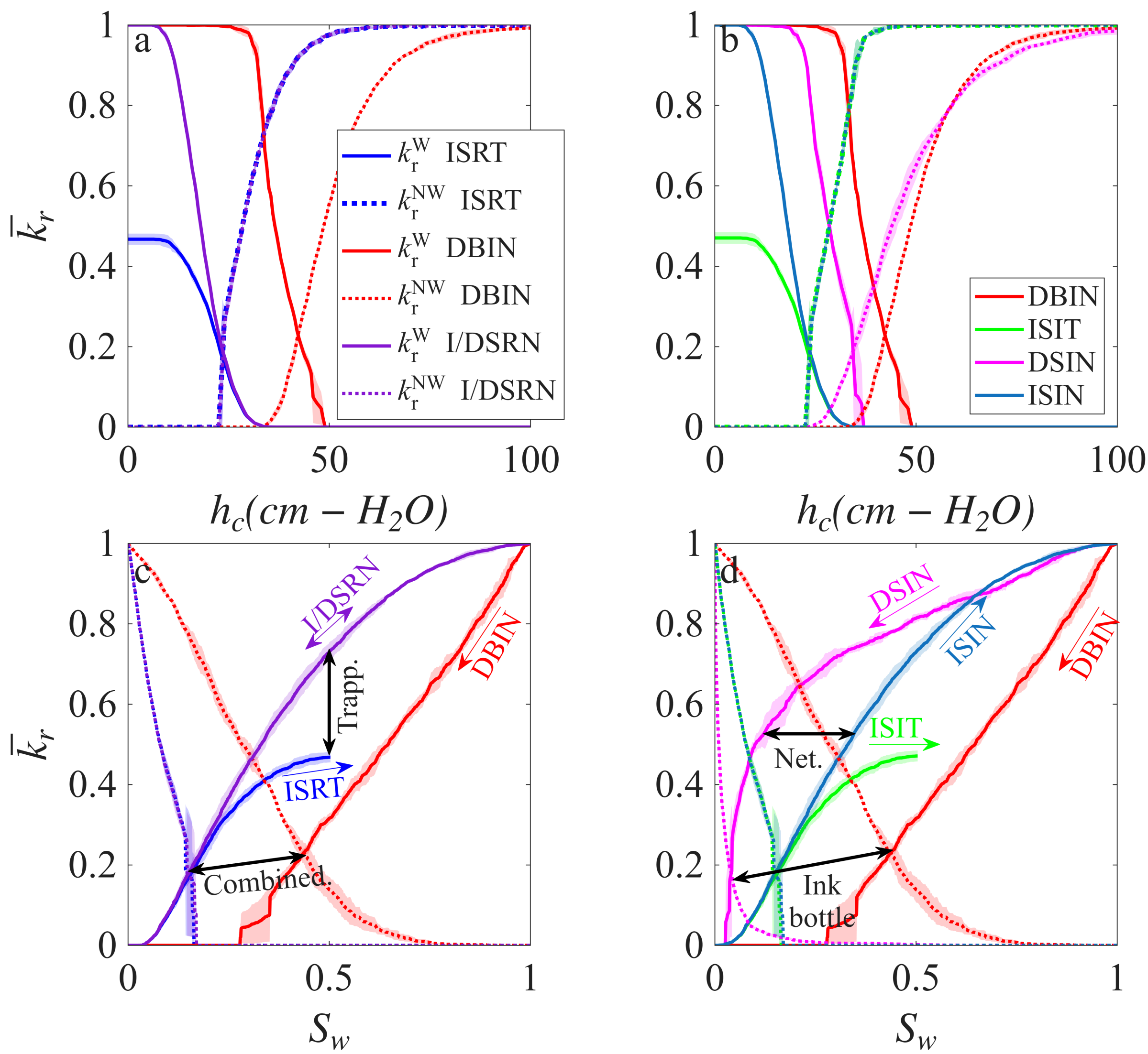

Figure 9. Relative permeability curves of the networks without correlation between the pore bodies' (r_s) and throats' (r_b) radii for the different displacement modes indicated in the legends.

https://doi.org/10.5194/egusphere-2026-4185
Preprint. Discussion started: 27 July 2026

3.4 Effect of network connectivity

3.4.1 Retention curve

The effect of the pore system connectivity on the retention curves (Fig. 10) is evaluated using a regular 18-neighborhood connected ("NN+2NN", Fig. 3a), irregular network with a mean coordination of $\bar{N}_c = 6$, without (Fig. 3b) and with (Fig. 3c) correlation between the pore connectivity (local N_c) and the pore body radius (r_s). Notice not to confuse the correlation analyzed in this section with the correlation described in the previous subsection between r_b and r_s. For all the cases evaluated in this section, r_s and r_b are correlated as specified in section 2.1.2.

Combined effects:

In general, the higher connectivity (Fig. 3a) and correlation between the pore N_c and r_s (Fig. 3c), narrow the hysteretic loop compared to the irregular not-correlated case (Fig. 3b) (Fig. 10). The reversible I/DSRN (purple line) retention curve is similar in all connectivity cases, because the sites are taken from a similar distribution. However, increasing connectivity shifts the breakthrough of the WP to a larger h_c and a lower S_w, and the disconnection of the NWP to a smaller h_c and larger S_w. This can be explained by the reduction in the percolation threshold with the increase in $\bar{N}_c$ (Hunt and Sahimi, 2017).

Comparing the retention curves with and without correlation between the pore size and its connectivity shows that the WP breakthrough of the correlated case is at a smaller h_c and higher S_w (suggesting a higher percolation threshold) than in the uncorrelated case (Fig. 10). In contrast, the disconnection of the NWP occurs at a smaller h_c and higher S_w in the correlated compared to the uncorrelated case, which suggests a lower percolation threshold of the NWP. This asymmetry can be explained by the filling order; during imbibition, the WP invades pores in increasing size order, thus the actual mean local N_c of the WP-filled pores is smaller than the mean $\bar{N}_c$ of the network, and the percolation threshold is larger. This is supported by the results of the p_{cs} at breakthrough in Figure A4 below. During drainage, the opposite occurs, where pores are drained from the largest (with the highest local N_c) to the smallest, resulting in actual mean local N_c of the WP-filled pores larger than the saturated network mean $\bar{N}_c$ and in a lower percolation threshold. For the uncorrelated case, the mean local N_c is similar to the global mean, $\bar{N}_c$ (up to some finite sample effect).

Comparing the combined effects hysteretic loop (DBIN-ISRT) of the irregular not-correlated lattice (Fig. 3c) to the simple-cubic one (Fig. 5c) shows a narrower loop at the low h_c values, but a much longer tail (at the high h_c) in the irregular network (Fig. 10). As expected, the retention curve of the ISRT in the highly connected lattice (blue lines in Fig. 10a) has a higher maximal S_w and a higher breakthrough h_c compared to the simple-cubic lattice (Fig. 5c). In contrast, the DBIN curve (red lines) of the highly connected lattice has a lower air breakthrough h_c and a larger S_w value compared to the simple cubic lattice. These effects result in a narrower hysteretic loop in the highly connected lattice. The ISRT retention curves of the irregular, not-correlated network (Fig. 10b) resemble the simple-cubic one. The DBIN retention curve (red line) in the irregular not-correlated network (Fig. 10b) has a wider span of h_c. When correlated (Fig. 10c), the span of h_c values narrows.

Trapping:

As expected, the highly connected pore system reduces the fraction of the entrapped resident phase. In accordance, the differences between ISRN and I/DSRT (and also between ISIN and ISIT) in highly connected networks (Fig. 10a) are smaller than in

https://doi.org/10.5194/egusphere-2026-4185
Preprint. Discussion started: 27 July 2026

the simple-cubic grid (Fig. 5c). Similarly to ISRT, the ISIT retention curve of the irregular, not-correlated network (Fig. 10e) resembles the simple-cubic one. However, when correlated, the maximal S_w value is higher (similar to the highly connected one). This is because when correlated, the larger pores are better connected and the resident phase is less likely to get trapped.

Ink-bottle hysteresis:

The lower air entry pressure value in DBIN for the highly connected networks narrows the hysteretic loop caused by the ink-bottle mechanism (DBIN vs DSIN, Fig. 10d). Unlike for the DBIN curve discussed above, the network irregularity does not affect the DSIN tailing (towards the high h_c values). Thus, for irregular networks, especially for the non-correlated ones, the ink-bottle hysteresis affects mostly the loop at the high h_c values.

Network hysteresis:

Increasing the pore system connectivity is expected to decrease the difference between invasion and random percolation (Fig. 10a), due to a more "organized" pore filling order. In our simple-cubic ($N_c = 6$) lattice base case, the IP and RP retention curves are already very similar, so this effect is not visible directly by comparing ISIT with ISRT (or I/DSRN with ISIN). However, the higher connectivity affects the hysteretic loop attributed to the network hysteresis mechanism (DSIN-ISIN), which is smaller for the high $\bar{N}_c$ (Fig. 10d) compared to the simple-cubic lattice (5d). Moreover, in the irregular network, the DSIN and ISIN curves (Fig. 10e and f) converge at a larger h_c than in the regular simple-cubic lattice (Fig. 5b), i.e., the $N_c - r_s$ correlation decreases the effect of the network hysteresis mechanism (Fig. 10f).

3.4.2 Permeability curves

Combined effects:

Similarly to the retention curves, the combined effects-hysteretic loops (ISRT-DBIN) of the permeability curves ($k_r(h_c)$), for both WP (solid lines) and NWP (dotted lines), are narrower in the highly connected pore system (Figure 11a) compared to the simple-cubic case (Fig. 6a). In addition, in the highly connected networks, the intersection points where $k_r^W(h_c) = k_r^{NW}(h_c)$ occur (for both ISRT and DBIN) in a larger k_r value (higher for DBIN compared to ISRT) and a lower h_c. Interestingly, the I/DSRN-DBIN hysteresis loop of the $k_r^W(S_w)$ curves in the regular highly connected ($N_c = 18$) networks (Fig. 11c) is wider than in the simple-cubic lattice ($N_c = 6$, Fig. 6c). In this, the curvatures of the DBIN and I/DSRN $k_r^W(S_w)$ curves are different in the highly connected networks, where DBIN has a negative curvature and I/DSRN a positive one, while in the simple-cubic case, the $k_r^W(S_w)$ curves are almost linear. For the NWP, the increased connectivity increases the disconnection S_w point ($k_r^{NW} = 0$) for the ISRT, but hardly affects the breakthrough ($k_r^{NW} = 0$) for DBIN, thus increasing the width of the $k_r^{NW}(S_w)$ hysteretic loop at lower S_w (where k_r^{NW} of ISRT > DBIN) and narrowing the loop in high S_w (where k_r^{NW} of DBIN > ISRT).

Unlike the increased connectivity case, the maximum ISRT k_r^W values of the irregular networks (of $\bar{N}_c = 6$) are similar to the simple-cubic case, slightly higher for the case with the correlation between N_c and r_s (Fig. 12 a and b). Similarly to the increase in connectivity, the irregular network with correlation, also widens the $k_r^W(S_w)$ hysteretic loop (Figure 12b) compared to the regular network (Fig. 6c), mostly because of the higher S_w in which trapping occurs (ISRT k_r^W reaches a plateau). Interestingly, in the non-correlated case (Fig. 12a), the $k_r^W(S_w)$ loop is much narrower than in the regular case (Fig. 6c). This suggests there are some counter-acting effects where the distribution of connections and the addition of the diagonal direction connections

https://doi.org/10.5194/egusphere-2026-4185
Preprint. Discussion started: 27 July 2026

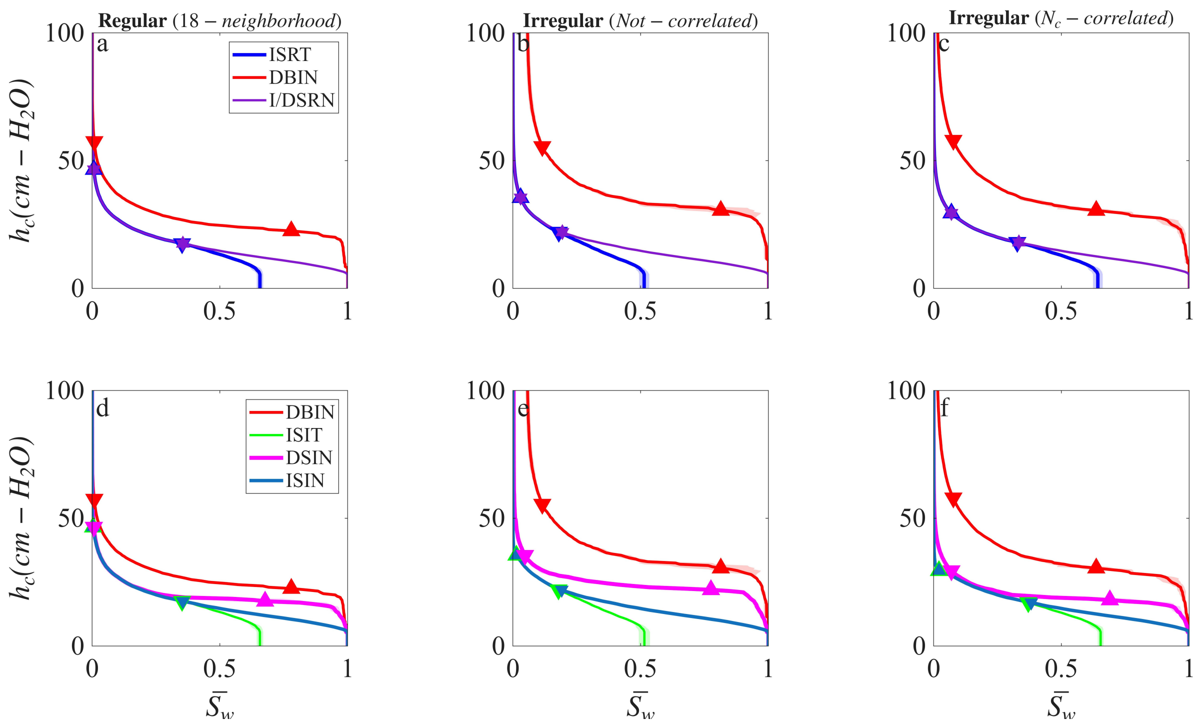

Figure 10. Retention curves of the different displacement modes (as indicated in the legends) in a regular 18-neighborhood lattice (a and d), irregular ($\bar{N}_c = 6$, b and e), and irregular with correlation between the pore connectivity and size (c and f).

reduce the effect of hysteresis on $k_r^W(S_w)$ curves, and, at the same time, the correlation between r_s and N_c increases the effect of hysteresis on $k_r^W(S_w)$.

Trapping:

As expected, and in agreement with the retention curves, the maximum k_r^W values of the cases with trapping (i.e., ISRT and ISIT) are larger in the highly connected lattice. This results in a smaller effect of trapping on the k_r^W and a completely negligible effect on the k_r^{NW} (Fig. 11b). The ISRT and ISIT in the irregular correlated case (Fig. 12b and d) have a slightly higher maximum k_r^W compared to the non-correlated case (Fig. 12a and c) and the regular simple-cubic case (Fig. 6c), obtained at a larger S_w (visible in the retention curve discussed above; Fig. 10b and e and c and f).

Ink-bottle hysteresis:

When increasing the coordination number, the effect of the ink-bottle hysteresis (DBIN-DSIN) increases for $k_r^W(h_c)$ (Fig. 11b) and decreases for $k_r^W(S_w)$ (Fig. 11d). Similar trends are observed for the NWP. Despite this observation, the ink bottle effect on the $k_r^W(S_w)$ and $k_r^{NW}(S_w)$ remains relatively small compared to other mechanisms (see Network hysteresis below).

The effect of the ink-bottle hysteresis on the $k_r^W(S_w)$ and $k_r^{NW}(S_w)$ in irregular networks (Fig. 12c and d) is mostly similar to that of in the regular simple-cubic case (Fig. 6d), while the non-correlated case has slightly wider loops for both WP and NWP at low S_w values.

https://doi.org/10.5194/egusphere-2026-4185
Preprint. Discussion started: 27 July 2026

Network hysteresis:

Compared to the simple-cubic network (Fig. 6b), the higher connectivity significantly widens the network hysteresis (ISIN-DSIN) loop of $k_{\mathrm{r}}^{W}(S_{\mathrm{w}})$ and $k_{\mathrm{r}}^{NW}(S_{\mathrm{w}})$ (Fig. 11d). This is somewhat counterintuitive, especially in light of the effect of connectivity on decreasing the $S_{\mathrm{w}}(h_{\mathrm{c}})$ network hysteresis discussed above. The explanation is that the increase in connectivity reduces the percolation threshold and increases the occupancy probability of the invading phase at the disconnection of the residing phase, thus allowing for a larger span of S_{w} with relative permeability larger than zero. In contrast, increasing the connectivity does not significantly affect the network hysteresis loop of $k_{\mathrm{r}}^{W}(h_{\mathrm{c}})$ and $k_{\mathrm{r}}^{NW}(h_{\mathrm{c}})$ curves (Fig. 11b).

The effect of network hysteresis on the irregular network without correlation (Fig. 12c) $k_{\mathrm{r}}^{W}(S_{\mathrm{w}})$ is similar to that of the regular simple-cubic lattice (Fig. 6d). Conversely, the correlated case (Fig. 12d) has a wider $k_{\mathrm{r}}^{W}(S_{\mathrm{w}})$ ISIN-DSIN loop. Interestingly, the opposite is observed for the NWP, where the uncorrelated case (Fig. 12c) has a wider $k_{\mathrm{r}}^{NW}(S_{\mathrm{w}})$ ISIN-DSIN loop compared to the correlated and regular cases.

3.5 Correspondence to the p_w and p_d functions of hysteresis models

Scaling functions of the main hysteresis loop (p_w, p_d) served in several models for predicting the internal scanning loops (which were not simulated in the present study). With a slight modification to the works of (Everett, 1955; Topp, 1971; Mualem and Dagan, 1975), a function p_d can be defined as the volume fraction of the pores which have emptied during drainage, relative to those which are yet to be filled during imbibition for a similar capillary head value (h_{c}).

$$p_d = \frac{1 - S^{W}_{drain}(h_{\mathrm{c}})}{1 - S^{W}_{imb}(h_{\mathrm{c}})} \tag{6}$$

where $S^{W}_{drain}(h_{\mathrm{c}})$ and $S^{W}_{imb}(h_{\mathrm{c}})$ are the corresponding WP saturation-capillary head functions of the drainage and imbibition processes.

Similarly, a function p_w can be defined as the volume fraction of the filled (imbibed) pores relative to those which are yet to be drained.

$$p_w = \frac{S^{W}_{imb}(h_{\mathrm{c}})}{S^{W}_{drain}(h_{\mathrm{c}})} \tag{7}$$

Figure 13 presents the p_d and p_w of the different networks properties (different lines) and for the different displacement modes (different panels). Fig. 13a presents the p_d and p_w when comparing ISRT to the reversible DSRN case (i.e., the draining of the pores from the largest to smallest). In this loop (ISRT-DSRN), the hysteresis is affected solely by the trapping of the NW-phase during ISRT (imbibition). In consequence, both p_d and p_w decrease with increasing S_{w}. Increasing the variability in the PSDs (from $CV = 0.2$ to 0.5 and to 1), causes a more pronounced decline in the p_w and p_d, starting at a lower S_{w} and ending with smaller minimum values of p_w. The irregular network without correlation between the size of the pore and its coordination number (light blue lines) is very similar to the simple-cubic case with similar mean coordination number and PSD variability (blue line). In comparison, when the coordination number is correlated ($N_c Corr$) to the pore size, or for a better connected pore system ($N_c = 18$), the decline in p_d and p_w are at larger S_{w} and to a larger minimum p_w value.

https://doi.org/10.5194/egusphere-2026-4185
Preprint. Discussion started: 27 July 2026

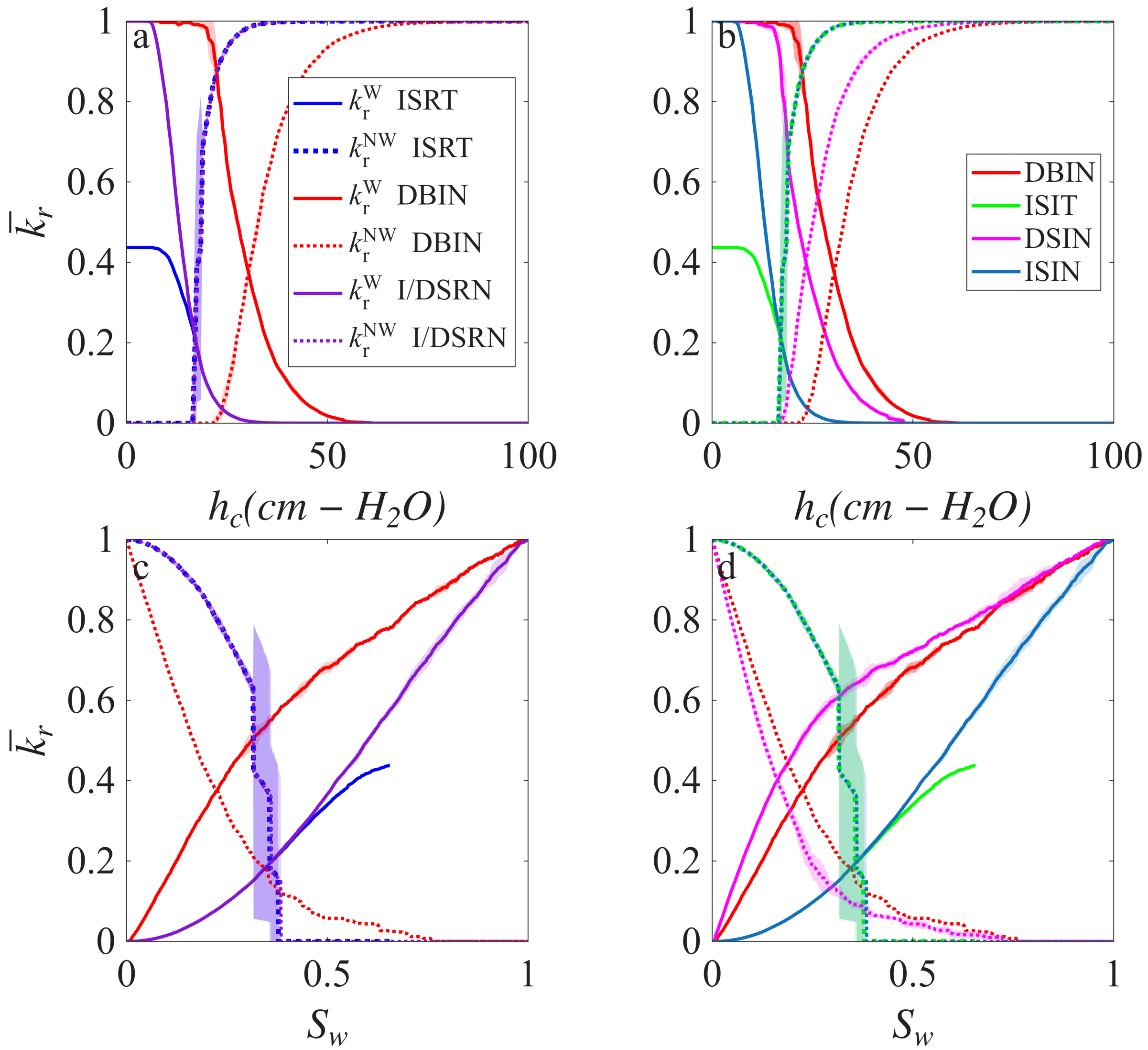

Figure 11. Relative permeability curves for the different displacement modes (as indicated in the legends) in a regular, 18-neighborhood-connected lattice.

770 The p_d (dashed lines) in the main drainage curve (DBIN, Fig. 13b) are almost linear with S_w. This suggests that there is very little overlap between the I/DSRN and DBIN retention curves, which can be explained by the shift caused via the ink-bottle effect. Similarly, p_w in this case is close to zero for most of S_w values (with the exception of the highly connected network). The same is observed when comparing the DBIN to ISRT instead of ISRN (Fig. 13c), illustrating the dominance of the ink-bottle effect on the hysteresis loop.

https://doi.org/10.5194/egusphere-2026-4185
Preprint. Discussion started: 27 July 2026

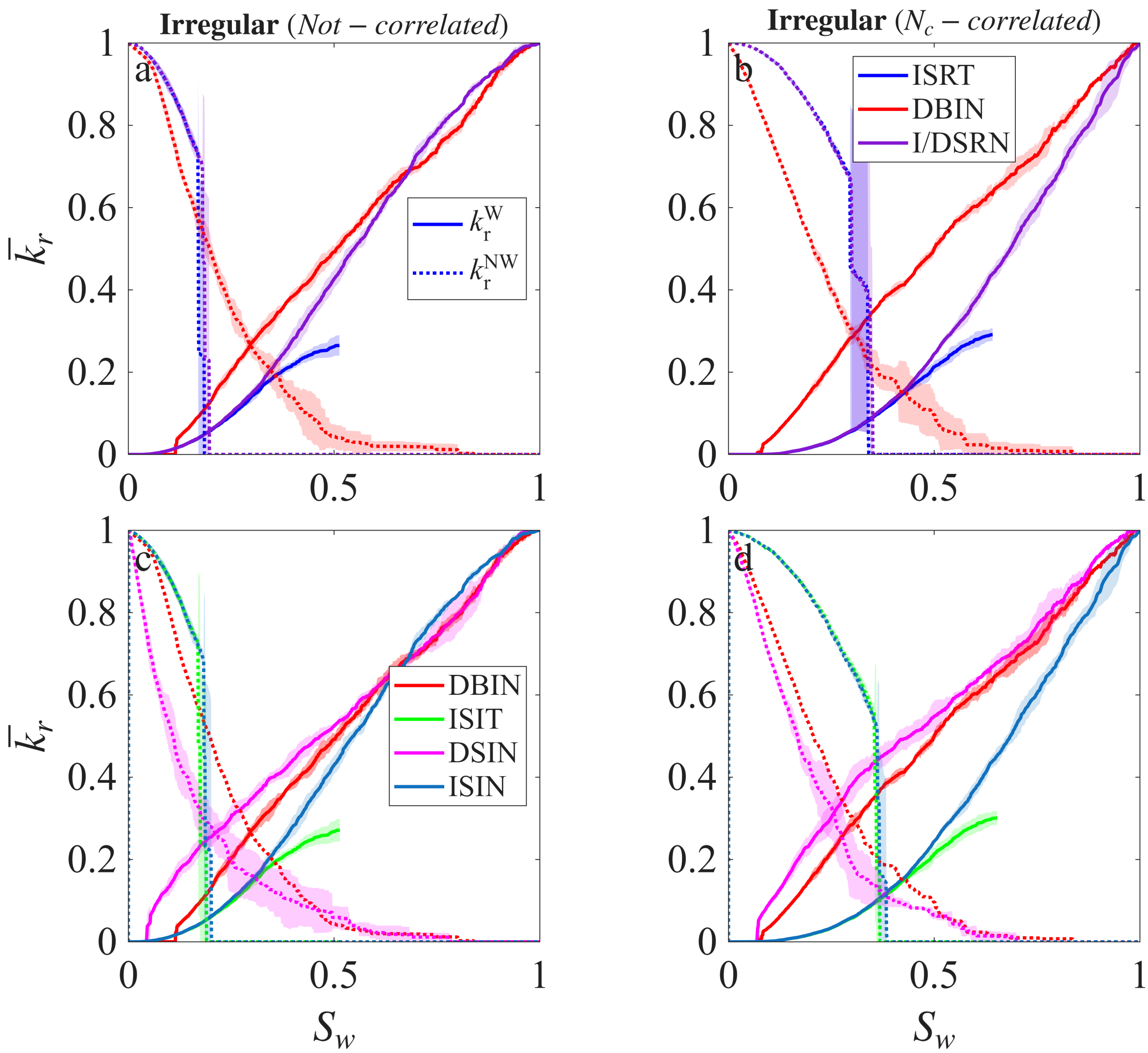

Figure 12. Relative permeability curves for the displacement modes (as indicated in the legends) in an irregular lattice without (left panels) and with (right panels) correlation between the pore's coordination number (N_c) and its size (r_s).

In contrast to the effect of trapping, the invasion percolation displacement mode, related to the network hysteresis, increases $p_w(S_w)$ in the ISIN-DSRN loop (Fig. 13d) and decreases $p_d(S_w)$ in the DSIN-ISRN loop (Fig. 13e). Interestingly, the ISIT-DSRN processes (Fig. 13e) presents a non-monotonic behavior of the p_w, suggesting that network hysteresis governs the p_w at low S_w, while trapping governs p_w at large S_w.

https://doi.org/10.5194/egusphere-2026-4185
Preprint. Discussion started: 27 July 2026

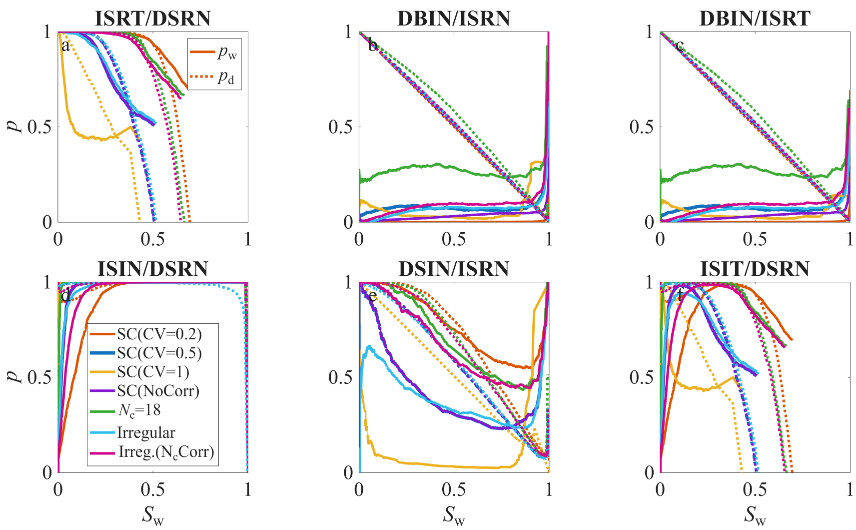

Figure 13. p_d (dashed line, Eq.6) and p_w (solid line, Eq.7) of the different network properties and lattice type: SC refers to simple-cubic lattice (Fig. 2a) with the different PSD-variation coefficients ($CV = 0.2$, 0.5 and 1, according to the PSDs in Fig. 1). Except for the two cases in which it is stated otherwise, the medium variability (CV=0.5) of the PSD is used. The SC (NoCorr) is the simple-cubic case but without correlation between r_s and r_b (Fig. 2b), $N_c = 18$ is the regular 18-neighbour-connected lattice (Fig. 3a), and finally the Irregular networks without (Fig.3b) and with (Irreg.(N_cCorr), Fig.3c) correlation between N_c and r_s. In all the panels except for panel "c", the non-hysteretic case I/DSRN (ISRN for drainage cases and DSRN for imbibition cases) was used as the reference case (reverse displacement). In panel "c", ISRT was used for the imbibition case and DBIN as the drainage one.

4 Conclusions

The magnitude (width) of the hysteretic loop and the shape of the different curves depend on the displacement processes and the pore systems properties. Different hysteresis mechanisms affect differently the retention ($S_w(h_c)$) and permeability ($k_r^W(S_w)$, $k_r^{NW}(S_w)$, $k_r^W(h_c)$ and $k_r^{NW}(h_c)$) curves. At the same time, the impacts of different displacement mechanisms are strongly affected by the pore system properties.

Retention curve:

For all the evaluated scenarios and pore system properties, the trapping of the resident phase below the percolation threshold (breakthrough) is negligible. This is explained by the relatively high connectivity of the pore system under evaluation ($\bar{N}_c = 6$ or higher). Interestingly, the saturation degree (S_w) and capillary head (h_c) at the disconnection point of the residing (NWP) are similar for the imbibition cases, with and without trapping. This suggests that most of the NWP trapping occurs at WP occupation probabilities higher than the disconnection threshold. As a result, trapping affects the retention curves at low h_c and high S_w. Decreasing the variation (spread) of the pore system and increasing its connectivity reduces the fraction of entrapped NWP. Conversely, irregular networks decrease the fraction of entrapped NWP only if there is correlation between the size and connectivity of the pores. In contrast to the trapping mechanism, the ink-bottle effect is not limited to high S_w and affects

https://doi.org/10.5194/egusphere-2026-4185
Preprint. Discussion started: 27 July 2026

the retention curves in the entire range of saturation degree. Increasing the variation of the pore size distribution dramatically mitigates the ink-bottle effect. This is due to the decrease in the "air entry" value and the increasing overlap between the r_s and r_b size distributions. Similarly to the increase in PSD variation, increasing the connectivity also mitigates the effect of the ink-bottle mechanism. In contrast, the effect of the network irregularity on the ink bottle mechanism is not significant. The effect of the network hysteresis is smaller at high and low h_c values. Unlike the ink-bottle mechanism, for which the main effect is a uniform right shift in the retention curve, the effect of the network hysteresis is not uniform, affecting the high S_w more than the low S_w values. Similarly to the factors affecting trapping, decreasing the variability of the network PSD and increasing its connectivity reduces the effect of the network hysteresis, where for irregular networks, network hysteresis decreases only if there is a correlation between the size and connectivity of the pores.

Relative permeability curves:

Trapping of the NWP dramatically affects the permeability of the WP, especially when the radii of the pore bodies and throats are correlated and distributed with a high variability. Increasing the pore systems connectivity or adding correlation between the pore sizes and their connectivity reduce the effect of trapping on the relative permeability curves. On the other hand, trapping has little effect on the NWP relative permeability curves. Similarly to the retention curves, increasing the variability in the PSD reduces the ink-bottle effect on the $k_\mathrm{r}(h_\mathrm{c})$ curves. The ink-bottle mechanism affects the $k_\mathrm{r}(h_\mathrm{c})$ curves, but has little effect on the $k_\mathrm{r}(S_\mathrm{w})$ curves (for both WP and NWP), provided that the r_s and r_b are correlated. In this context, a hysteretic $k_\mathrm{r}(S_\mathrm{w})$ curve in which the drainage k_r^W curve is lower than the imbibition one might suggest that the pore system geometry cannot be described with size-correlated pore throats and bodies. In contrast, a hysteretic $k_\mathrm{r}(S_\mathrm{w})$ curve in which the drainage k_r^W curve is larger than the imbibition one suggests strong network hysteresis. In turn, the network hysteresis effect on the $k_\mathrm{r}(S_\mathrm{w})$ increases with pore system connectivity and with correlation between the pore size and its connectivity.

The similarities between DSIN and DBIN (ink-bottle effect) and ISIN and I/DSRN (percolation mode effect) suggest that network hysteresis (DSIN-ISIN) is responsible for the hysteresis of $k_\mathrm{r}(S_\mathrm{w})$ at low S_w, and that trapping (ISIT-ISIN) is the main hysteretic mechanism for high S_w. This explains why the hysteretic behavior in $k_\mathrm{r}(S_\mathrm{w})$ is not reported in many studies that disregard the network hysteresis. This also means that the $k_\mathrm{r}(S_\mathrm{w})$ curve holds information about the network hysteresis mechanism, which is expected to be strongly affected by the pore system connectivity.

The relative permeabilities intersection points ($k_\mathrm{r}^W = k_\mathrm{r}^{NW}$) of the drainage cases (DBIN and DSIN) occur at higher k_r, h_c, and S_w values compared to the imbibition cases. The k_r values at the intersection points are related to the network hysteresis mechanism (DSIN-ISIN), while the h_c and, to a smaller extent, the S_w values at the intersection points are also related to the ink-bottle mechanism (DSIN-DBIN). During drainage via IP, small pores protect larger pores (connected with better conducting throats) from being drained, thus keeping a higher conductance backbone for the WP than in the imbibition case. During imbibition, the NWP maintains a considerable permeability value until disconnection.

https://doi.org/10.5194/egusphere-2026-4185
Preprint. Discussion started: 27 July 2026

Appendix A: Lattice size effects

The effect of the network size and the effect of periodic vs confined (impermeable) boundaries were evaluated in a sensitivity analysis. The periodic conditions in the faces perpendicular to the main flow direction are obtained by appending additional bonds that connect the right-and-left and top-and-bottom faces. In this analysis, for each domain size (in the range $5 \leq N \leq 33$), five realizations were used for each size (and scenario), the r_s and r_b were sampled from the same log-normal distribution of the "medium" variability described above. Then, the intrinsic permeability (of the saturated simple-cubic lattice) was calculated. Figure A1 presents the effect of the lattice size (number of sites in each direction) on the evaluated mean intrinsic permeability ($k_t extrms$) in confined (black) and periodic (red) domains and the mean pore volume ($V_t extrms$, blue) of all the sites designated with a distributed $r_t extrms$. The slightly larger permeability of the periodic domain for small lattices can be explained by the additional bonds, even if they are oriented in the perpendicular direction to the main flow. Interestingly, the periodic domain did not reduce (and even increased) the variability of the permeability (shaded regions in Fig. A1a) or the coefficient of variation (Fig. A1b), thus, we did not use the periodic condition in our analysis.

The permeability decreases with the lattice size (Fig. A1a). The reduction in permeability with the lattice size is well documented (Friedman and Seaton, 1996; Wilkinson, 1986). This observation is consistent with the effect of the lattice size in decreasing the percolation threshold (Sahimi, 2011; Wilkinson, 1986). Hunt and Sahimi (2017) explained the size dependence of the macroscopic properties through the transition from statistically self-similar to a macroscopically homogeneous statistics. For (a trivial) illustration, for the smallest possible $3D$ simple-cubic bond lattice of 6 bonds (2 in each main direction passing through a single junction), the percolation threshold is 0.2 (1/5), well below the theoretical value of 0.249. A smaller percolation threshold suggests a higher permeability for a given occupation probability.

Unlike the permeability, the lattice size does not affect the mean of the sampled $r_t extrms$, but rather just its standard deviation. Resulting in oscillations around the expected mean pore volume. Interestingly, the variability of the mean pore volume converges at the same rate as that of the permeability (Fig. A1b). This indicates that convergence to the mean porosity is a good quantifier of the representative elementary volume (REV) (Bear, 2012).

The interaction between the effects of the different network properties and the lattice size is evaluated in Figure A2. Increasing the variability in the PSD reduces k_s; the effect of lattice size (the reduction of k_s with increasing N discussed above) is significant at low and medium variances, but not at high variability, probably because of the limited number of realizations. The correlation between the neighboring bonds' geometrical mean and sites' radii increases k_s, this is because a site with a large r_s is more likely to have highly conducting bonds; these small-scale (6-bonds) spatial correlations result in larger (L-size) spatial correlations that form preferential pathways. The highly connected pore system ($N_c = 18$) are much more conducting because of the dual effect of more conducting bonds and better connectivity, allowing better preferential paths. The k_s values of the regular and irregular networks with the same mean coordination number ($\bar{N}_c$) are very similar, in accordance with the literature (Sahimi, 2011). In addition, as expected, the correlation between N_c and r_s increases k_s. This is to be expected because the correlation forms spatially correlated preferential paths, where higher pores (large r_s) are connected to more conducting bonds (large r_b), and are also better connected (high N_c).

https://doi.org/10.5194/egusphere-2026-4185
Preprint. Discussion started: 27 July 2026

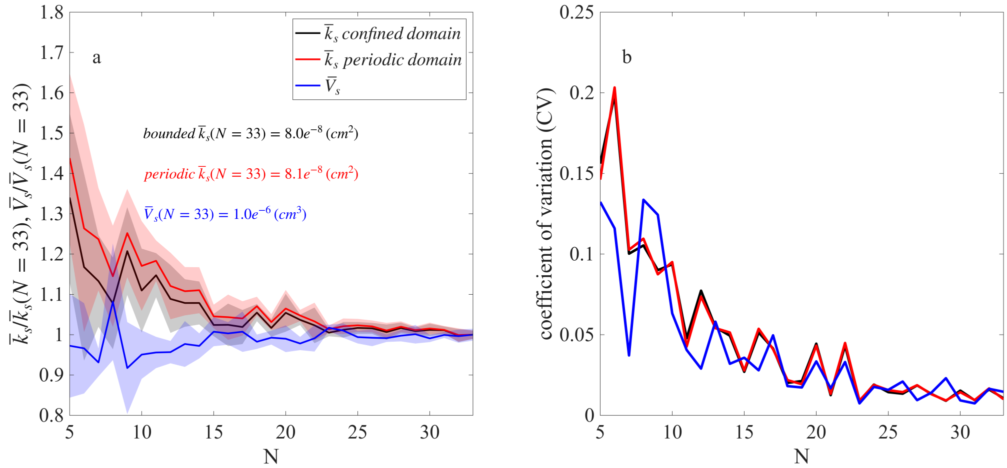

Figure A1. Effect of the lattice size (N) on the (a) intrinsic permeability (k_s) in confined (black) and periodic (red) domains and mean pore volume (V_s, blue), and (b) their coefficient of variation. The colored area represents the standard deviation between the five realizations used for each lattice size in this analysis.

In addition to the sensitivity analysis conducted on the intrinsic permeability, the two main scenarios (ISRT and DBIN) were evaluated on a $20 \times 20 \times 20$ lattice (Figure A3). The similarities in the retention (top panels) and permeability ($k_\mathrm{r}(h_\mathrm{c})$, bottom panels) curves between the $N = 20$ and $N = 15$, even for the high CV cases (c and f), indicate that the effect of the finite lattice size is negligible, except for a few aspects. For example, the effect of trapping of the NWP during imbibition (ISRT) increases with N increasing from 15 to 20.

Another size-dependent difference is in the breakthrough saturation-capillary head values of the invasion percolation scenarios (e.g., DBIN). It should be mentioned that this is an inherent significant difference between RP and IP (Wilkinson and Willemsen, 1983). However, as seen in Figure A3, this does not affect the retention curve and only slightly affects the $k_\mathrm{r}(h_\mathrm{c})$ curves. However, as this effect is shared in all the IP cases, it does not change the insights and conclusions presented in this work.

The percolation threshold is one of the most basic properties of a conducting network. The proximity of the percolation values to the previously determined values suggests that the lattice and flow type models are reliable and that the size effect is not a source of significant bias. The random site percolation threshold of a simple-cubic lattice is about 0.3115 (Wang et al., 2013), indicated by the dashed black line in Figure A4. It can be seen that the mean p_cs of the RP cases (ISRT and ISRN, "ISR") of the simple cubic (Fig. A4a) are centered near this value regardless of the variability in the PSD. It can also be seen that the irregular network without correlation with a mean coordination number $\bar{N}_\mathrm{c} = 6$ (green, right-hand side panel) is also very similar to the literature value. The literature value of the 18-neighbor (simple-cubic + NN + 2NN) lattice is 0.137 (Kurzawski and Malarz, 2012), which is within the range obtained in our analysis for the ISR (purple box in Fig. A4b) of 0.148 ± 0.016. Moreover, the high percolation threshold of the irregular with pore-size-connectivity correlation network (ca. 0.475, blue) supports the

https://doi.org/10.5194/egusphere-2026-4185
Preprint. Discussion started: 27 July 2026

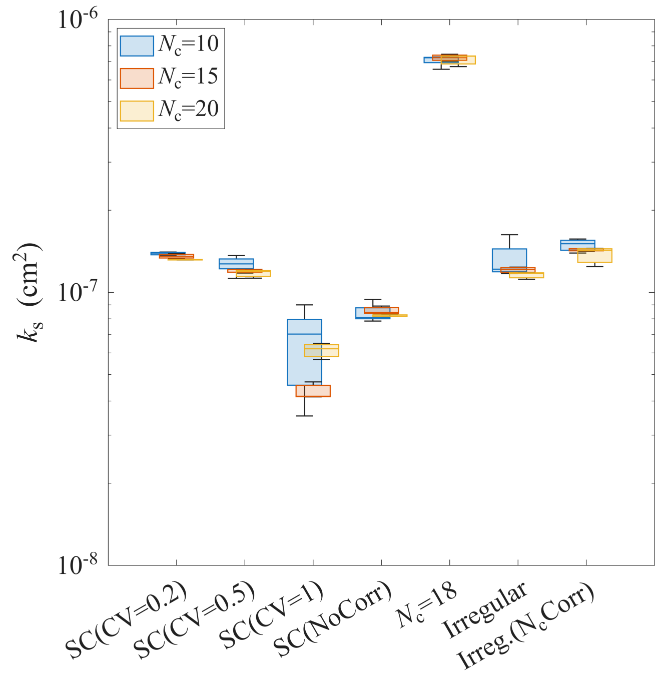

Figure A2. The intrinsic (single phase-saturated) permeability (k_s) dependence on the network properties and lattice size: SC refers to a simple-cubic lattice (Fig. 2a) with the different PSD-variation coefficients ($CV = 0.2$, 0.5 and 1, according to the PSDs in Fig. 1). For the other three cases the medium variability ($CV = 0.5$) of the PSD is used. The SC (NoCorr) is the simple-cubic case but without correlation between r_s and r_b (Fig. 2b), $N_c = 18$ is the regular 18-neighbour-connected lattice (Fig. 3a), and the Irregular networks without (Fig.3b) and with (Irreg.($N_c Corr$), Fig.3c) correlation between N_c and r_s.

explanation given here for the asymmetry in the effect of the correlation on the WP breakthrough and NWP disconnection points.

As mentioned above, the site invasion percolation threshold is size dependent. Wilkinson and Willemsen (1983) found values of 0.2 for $N = 10$ and a power law with an exponent of -0.48, suggesting that a $N = 15$, simple-cubic lattice should have a percolation threshold of $p_{cs} \approx 0.165$. In our analysis, lower values were obtained, which can be explained by some differences from the work described by Wilkinson and Willemsen (1983), namely the boundary conditions at the inlet. Wilkinson and Willemsen (1983) used a twice as long lattice in the flow direction (2N) and analyzed only the central part, while our values are obtained in the entire lattice, including the inlet face. Comparing the percolation thresholds of different lattice sizes (Figure A5) shows that the RP value does not change much with the increase of the lattice and that the slight reduction in the IP p_{cs} is consistent, further supporting the usability of the $N = 15$ lattice in this work.

https://doi.org/10.5194/egusphere-2026-4185
Preprint. Discussion started: 27 July 2026

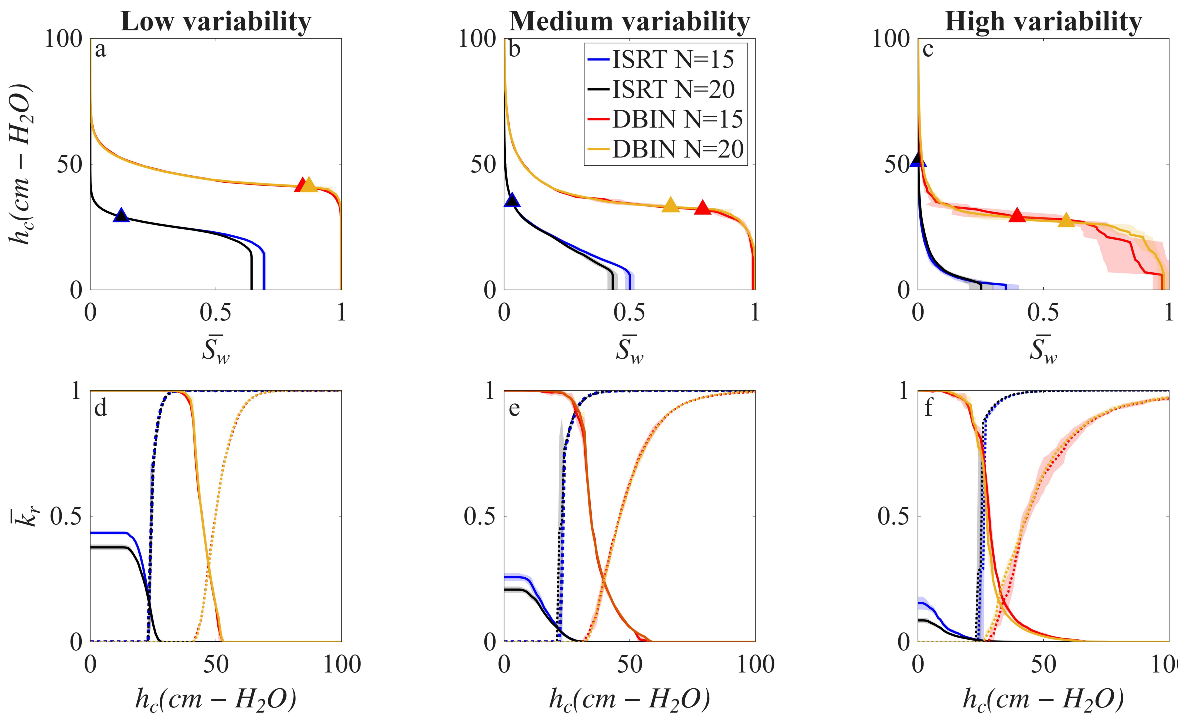

Figure A3. The retention (a-c) and permeability (d-f) curves of the low (a, d), medium (b, e), and high (c, f) PSD-variation for the $N = 15$ (ISRT in blue and DSIN in red) and $N = 20$ (ISRT in black and DSIN in orange) lattices. The breakthrough points are indicated in the retention curves with a Δ symbol.

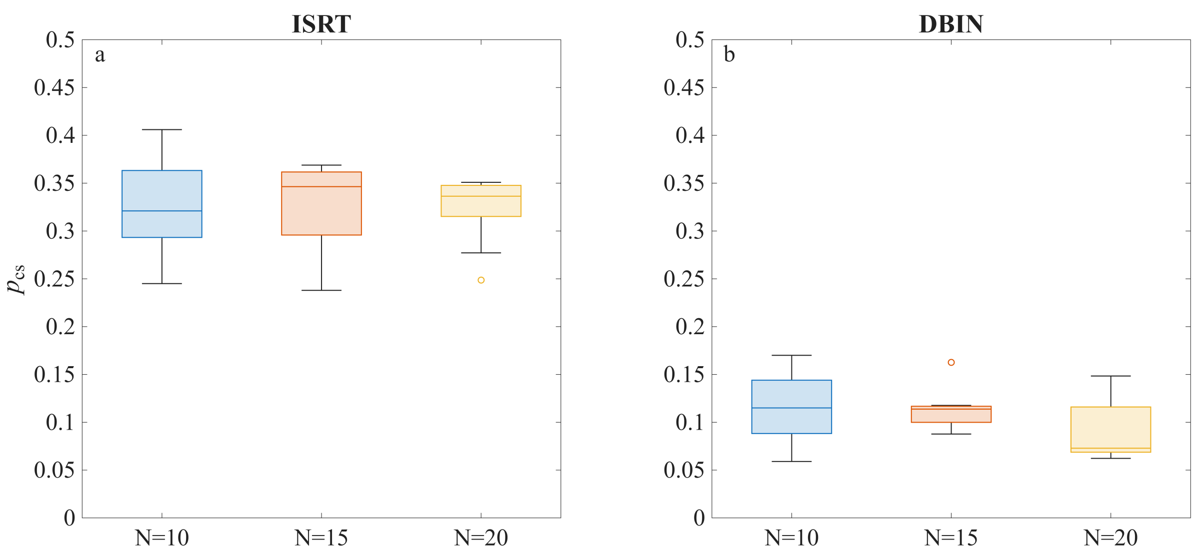

Figure A5. The effect of lattice size on the site percolation threshold for ISRT (a) and DBIN (b). The data in the boxplots includes all realizations and the three PSD-variability cases evaluated (the number of realizations are: $N_{N=10} = 15$, $N_{N=15} = 9$, $N_{N=20} = 9$).

https://doi.org/10.5194/egusphere-2026-4185
Preprint. Discussion started: 27 July 2026

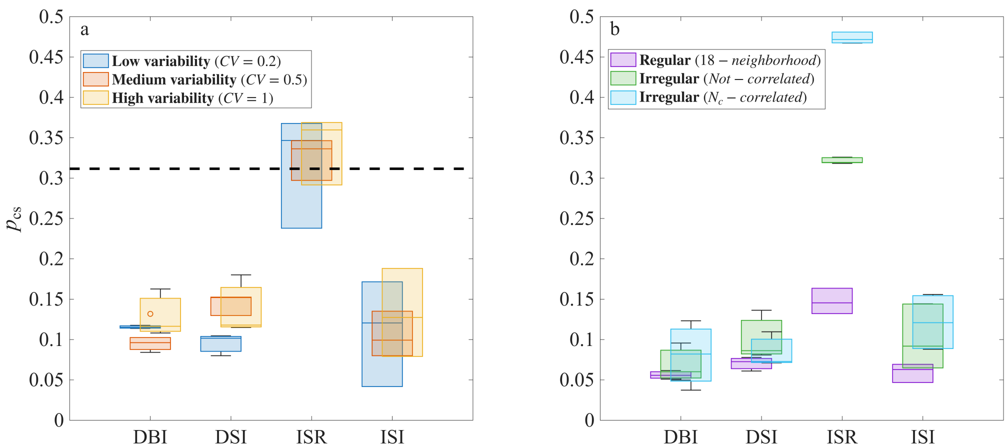

Figure A4. The occupancy probability (p_{cs}) at percolation (breakthrough) for the different displacement modes for a) different PSD-variability, and b) different pore system connectivity. The data in the boxplots includes all realizations and combines cases with and without trapping (e.g., ISR includes ISIT and ISIN), that is for the low and high variability and also for the highly connected and irregular networks the number of realizations is $N_{DBI} = N_{DSI} = 3$ and $N_{ISR} = N_{ISI} = 6$, while for the medium PSD-variability the number of realizations is doubled.

Author Contribution

Ben-Noah I. was in charge of: conceptualization, formal analysis, funding acquisition, developing and designing the methodology, programming and software development, creating data presentations, and writing the original draft, while Friedman S.P. and Mualem Y. reviewed & edited the manuscript

Code and Data Availability

The datasets and model codes in MATLAB formats (.mat and .m files) are available upon request.

Acknowledgements

This work is dedicated in honor of Dr. Ferenc (Franz) Preisach and his cardinal contribution to the understanding of hysteresis. This study was supported by the Israel Science Foundation through the grant number 1619/24.

Competing Interests

There are no competing interests.

https://doi.org/10.5194/egusphere-2026-4185
Preprint. Discussion started: 27 July 2026

References

Ambegaokar, V., Halperin, B., and Langer, J.: Hopping conductivity in disordered systems, Physical review B, 4, 2612, 1971.

Assouline, S. and Or, D.: Conceptual and parametric representation of soil hydraulic properties: A review, Vadose Zone Journal, 12, vzj2013–07, 2013.

Assouline, S. and Rouault, Y.: Modeling the relationships between particle and pore size distributions in multicomponent sphere packs: Application to the water retention curve, Colloids and Surfaces A: Physicochemical and Engineering Aspects, 127, 201–210, 1997.

Avraam, D. and Payatakes, A.: Flow regimes and relative permeabilities during steady-state two-phase flow in porous media, Journal of fluid mechanics, 293, 207–236, 1995.

Bear, J.: Hydraulics of groundwater, Courier Corporation, 2012.

Ben Noah, I. and Friedman, S. P.: Continuum modeling of steady air injection into partially saturated soils, Vadose Zone Journal, 14, vzj2014–12, 2015.

Ben-Noah, I., Friedman, S. P., and Berkowitz, B.: Dynamics of Air Flow in Partially Water-Saturated Porous Media, Reviews of Geophysics, p. e2022RG000798, 2023.

Ben-Noah, I., Hidalgo, J. J., and Dentz, M.: Pore network models to determine the flow statistics and structural controls for single-phase flow in partially saturated porous media, Advances in Water Resources, 193, 104 809, 2024a.

Ben-Noah, I., Hidalgo, J. J., and Dentz, M.: Singular value decomposition for single-phase flow and cluster identification in heterogeneous pore networks, Advances in Water Resources, 192, 104 779, 2024b.

Blunt, M.: An empirical model for three-phase relative permeability, SPE J., 5, 435, 2000.

Blunt, M. J.: Multiphase flow in permeable media: A pore-scale perspective, Cambridge university press, 2017.

Braun, E. and Holland, R.: Relative permeability hysteresis: laboratory measurements and a conceptual model, SPE Reservoir Engineering, 10, 222–228, 1995.

Butcher, P.: Effective medium treatments of random simple square and simple cubic conductance networks, J. Phys. C, 8, L324, 1975.

Chandler, R., Koplik, J., Lerman, K., and Willemsen, J. F.: Capillary displacement and percolation in porous media, Journal of Fluid Mechanics, 119, 249–267, 1982.

Chatzis, I. and Dullien, F.: Application of the theory of percolation for a model of drainage in porous media and relative permeability of injected non-wetting fluids, Oil Gas Sci. Technol. Rev. IFP, 37, 183, 1982.

Chatzis, I. and Dullien, F. A.: Modelling pore structure by 2-D and 3-D networks with applicationto sandstones, Journal of Canadian Petroleum Technology, 16, 1977.

Chatzis, I. and Dullien, F. A.: The modeling of mercury porosimetry and the relative permeability of mercury in sandstones using percolation theory, Int. Chem. Eng.;(United States), 25, 1985.

Diamantopoulos, E. and Durner, W.: Closed-form model for hydraulic properties based on angular pores with lognormal size distribution, Vadose Zone Journal, 14, vzj2014–07, 2015.

Dias, M. and Payatakes, A.: Network models for two-phase flow in porous media. Part 1. Immiscible microdisplacement of non-wetting fluids, J. Fluid Mech., 164, 305, 1986.

Dias, M. M. and Wilkinson, D.: Percolation with trapping, Journal of Physics A: Mathematical and General, 19, 3131, 1986.

Diaz, C., Chatzis, I., and Dullien, F.: Simulation of capillary pressure curves using bond correlated site percolation on a simple cubic network, Transport in Porous media, 2, 215–240, 1987.

Everett, D. H.: A general approach to hysteresis. Part 4. An alternative formulation of the domain model, Transactions of the Faraday Society, 51, 1551–1557, 1955.

Fatt, I.: The network model of porous media, Transactions of the AIME, 207, 144–177, 1956.

Friedman, S. P.: Dynamic contact angle explanation of flow rate-dependent saturation-pressure relationships during transient liquid flow in unsaturated porous media, Journal of adhesion science and technology, 13, 1495–1518, 1999.

Friedman, S. P. and Seaton, N. A.: On the transport properties of anisotropic networks of capillaries, Water Resources Research, 32, 339–347, 1996.

Friedman, S. P. and Seaton, N. A.: Critical path analysis of the relationship between permeability and electrical conductivity of three-dimensional pore networks, Water Resources Research, 34, 1703–1710, 1998.

Fu, Y., Liao, H., Chai, X., Li, Y., and Lv, L.: A hysteretic model considering contact angle hysteresis for fitting soil-water characteristic curves, Water Resources Research, 57, 2021.

Haines, W. B.: Studies in the physical properties of soil. V. The hysteresis effect in capillary properties, and the modes of moisture distribution associated therewith, The Journal of Agricultural Science, 20, 97–116, 1930.

Heiba, A., Sahimi, M., Scriven, L., and Davis, H.: Percolation theory of two-phase relative permeability, SPE reservoir engineering, 7, 123–132, 1992.

Heinse, R., Jones, S. B., Tuller, M., Bingham, G. E., Podolskiy, I., and Or, D.: Providing optimal root-zone fluid fluxes: effects of hysteresis on capillary-dominated water distributions in reduced gravity, Tech. rep., SAE Technical Paper, 2009.

Honarpour, M. and Mahmood, S.: Relative-permeability measurements: An overview, Journal of petroleum technology, 40, 963–966, 1988.

Hunt, A. G. and Sahimi, M.: Flow, transport, and reaction in porous media: Percolation scaling, critical-path analysis, and effective medium approximation, Reviews of Geophysics, 55, 993–1078, 2017.

Jarrell, P.: Practical Aspects of CO2 Flooding, Society of Petroleum Engineers, Richardson, TX, USA, 2002.

Jerauld, G. and Salter, S.: The effect of pore-structure on hysteresis in relative permeability and capillary pressure: pore-level modeling, Transport in porous media, 5, 103–151, 1990.

Joekar-Niasar, V., Hassanizadeh, S. M., and Dahle, H.: Non-equilibrium effects in capillarity and interfacial area in two-phase flow: dynamic pore-network modelling, Journal of fluid mechanics, 655, 38–71, 2010.

Knackstedt, M. A., Sheppard, A. P., and Pinczewski, W.: Simulation of mercury porosimetry on correlated grids: Evidence for extended correlated heterogeneity at the pore scale in rocks, Physical review E, 58, R6923, 1998.

Knackstedt, M. A., Sheppard, A. P., and Sahimi, M.: Pore network modelling of two-phase flow in porous rock: the effect of correlated heterogeneity, Advances in Water Resources, 24, 257–277, 2001.

Koplik, J.: Creeping flow in two-dimensional networks, J. Fluid Mech., 119, 219, 1982.

Koplik, J., Banavar, J., and Willemsen, J.: Molecular dynamics of Poiseuille flow and moving contact lines, Phys. Rev. Lett., 60, 1282, 1988.

Kurzawski, Ł. and Malarz, K.: Simple cubic random-site percolation thresholds for complex neighbourhoods, Reports on mathematical physics, 70, 163–169, 2012.

Laroussi, C. and De Backer, L.: Relations between geometrical properties of glass beads media and their main ψ (θ) hysteresis loops, Soil Science Society of America Journal, 43, 646–650, 1979.

Larson, R., Davis, H., and Scriven, L.: Displacement of residual nonwetting fluid from porous media, Chemical Engineering Science, 36, 75–85, 1981a.

https://doi.org/10.5194/egusphere-2026-4185
Preprint. Discussion started: 27 July 2026

Larson, R., Scriven, L., and Davis, H.: Percolation theory of two phase flow in porous media, Chemical Engineering Science, 36, 57–73, 1981b.

Lenormand, R., Zarcone, C., and Sarr, A.: Mechanisms of the displacement of one fluid by another in a network of capillary ducts, Journal of Fluid Mechanics, 135, 337–353, 1983.

Liu, H., Zhang, L., and Seaton, N. A.: Analysis of sorption hysteresis in mesoporous solids using a pore network model, Journal of colloid and interface science, 156, 285–293, 1993a.

Liu, H., Zhang, L., and Seaton, N. A.: Sorption hysteresis as a probe of pore structure, Langmuir, 9, 2576–2582, 1993b.

Mohanty, K. K. and Salter, S. J.: Multiphase flow in porous media: II. Pore-level modeling, in: SPE Annual Technical Conference and Exhibition?, pp. SPE–11 018, SPE, 1982.

Mualem, Y.: Modified approach to capillary hysteresis based on a similarity hypothesis, Water Resources Research, 9, 1324–1331, 1973.

Mualem, Y.: A conceptual model of hysteresis, Water resources research, 10, 514–520, 1974.

Mualem, Y.: A modified dependent-domain theory of hysteresis, Soil science, 137, 283–291, 1984.

Mualem, Y.: Hydraulic conductivity of unsaturated soils: Prediction and formulas, Methods of Soil Analysis: Part 1 Physical and Mineralogical Methods, 5, 799–823, 1986.

Mualem, Y. and Dagan, G.: A dependent domain model of capillary hysteresis, Water Resources Research, 11, 452–460, 1975.

Mualem, Y. and Miller, E.: A hysteresis model based on an explicit domain-dependence function, Soil Science Society of America Journal, 43, 1067–1073, 1979.

Naar, J., Wygal, R., and Henderson, J.: Imbibition relative permeability in unconsolidated porous media, Society of Petroleum Engineers Journal, 2, 13–17, 1962.

Néel, L.: Théorie des lois d'aimantation de Lord Rayleigh et les déplacements d'une paroi isolée, Cahiers de physique, 12, 1–20, 1942.

Onody, R. N., Posadas, A., and Crestana, S.: Experimental studies of the fingering phenomena in two dimensions and simulation using a modified invasion percolation model, Journal of Applied Physics, 78, 2970–2976, 1995.

Piri, M. and Blunt, M. J.: Three-phase threshold capillary pressures in noncircular capillary tubes with different wettabilities including contact angle hysteresis, Physical Review E—Statistical, Nonlinear, and Soft Matter Physics, 70, 061 603, 2004.

Piri, M. and Blunt, M. J.: Three-dimensional mixed-wet random pore-scale network modeling of two-and three-phase flow in porous media. II. Results, Physical Review E—Statistical, Nonlinear, and Soft Matter Physics, 71, 026 302, 2005a.

Piri, M. and Blunt, M. J.: Three-dimensional mixed-wet random pore-scale network modeling of two-and three-phase flow in porous media. I. Model description, Physical Review E—Statistical, Nonlinear, and Soft Matter Physics, 71, 026 301, 2005b.

Poiseuille, J. L. M.: Recherches sur les causes du mouvement du sang dans les vaisseaux capillaires, vol. 7, Impr. royale, 1839.

Poulovassilis, A.: The effect of the entrapped air on the hysteresis curves of a porous body and on its hydraulic conductivity, Soil Science, 109, 154–162, 1970.

Preisach, F.: Über die magnetische Nachwirkung, Zeitschrift für physik, 94, 277–302, 1935.

Raoof, A. and Hassanizadeh, S. M.: A new method for generating pore-network models of porous media, Transport in porous media, 81, 391–407, 2010.

Reis, P. and Måløy, K. J.: Drainage front width in a three-dimensional random porous medium under gravitational and capillary effects, Physical Review Research, 7, 033 244, 2025.

Sahimi, M.: Flow and transport in porous media and fractured rock: from classical methods to modern approaches, John Wiley & Sons, 2011.

https://doi.org/10.5194/egusphere-2026-4185
Preprint. Discussion started: 27 July 2026

Sahimi, M., Hashemi, M., and Ghassemzadeh, J.: Site-bond invasion percolation with fluid trapping, Physica A: Statistical Mechanics and its Applications, 260, 231–243, 1998.

Topp, G.: Soil-water hysteresis measured in a sandy loam and compared with the hysteretic domain model, Soil Science Society of America Journal, 33, 645–651, 1969.

Topp, G.: Soil-water hysteresis: The domain theory extended to pore interaction conditions, Soil Science Society of America Journal, 35, 219–225, 1971.

Wall, G. and Brown, R.: The determination of pore-size distributions from sorption isotherms and mercury penetration in interconnected pores: The application of percolation theory, Journal of colloid and interface science, 82, 141–149, 1981.

Wang, J., Zhou, Z., Zhang, W., Garoni, T. M., and Deng, Y.: Bond and site percolation in three dimensions, Physical Review E—Statistical, Nonlinear, and Soft Matter Physics, 87, 052 107, 2013.

Wilkinson, D.: Percolation model of immiscible displacement in the presence of buoyancy forces, Physical Review A, 30, 520, 1984.

Wilkinson, D.: Percolation effects in immiscible displacement, Physical Review A, 34, 1380, 1986.

Wilkinson, D. and Willemsen, J. F.: Invasion percolation: a new form of percolation theory, Journal of physics A: Mathematical and general, 16, 3365, 1983.

Yu, L., Laidlaw, W. G., and Wardlaw, N. C.: Sensitivity of drainage and imbibition to pore structures as revealed by computer simulation of displacement process, Advances in Colloid and Interface Science, 26, 1–68, 1986.

Zhou, A.-N.: A contact angle-dependent hysteresis model for soil–water retention behaviour, Computers and Geotechnics, 49, 36–42, 2013.